A Hierarchical Space-Time spectral element method for simulating complex multiphase flows

Mark Sussman

December 18-20, 2018, Tel Aviv. Advances in Applied Mathematics. A conference in memoriam of Professor Saul Abarbanel.

Motivation

- The Research for the space-time spectral element method was performed by Chaoxu Pei under the supervision of Mark Sussman and M. Yousuff Hussaini.
- We have discovered that the space-time spectral element method preserves structure in complex flow better than low order methods.
- We have discovered that it is easier than one might expect to extend a low order method to a space-time spectral method that is robust.
- Possible future applications: Stability Analysis in complex Multiphase Flow, vorticity confinement in complex multiphase and multimaterial flows, numerical methods with excellent dispersion relation preserving properties.

Wing Tip Vortices

Stability of Rotating Viscous and Inviscid Flows

Stability of Rotating Viscous and Inviscid flows

Hua-Shu Dou

Temasek Laboratories,
National Wind Tunnel Building
National University of Singapore,
Singapore 117508, SINGAPORE
Email: tsldh@nus.edu.sg; huashudou@yahoo.com

Abstract: Flow instability and turbulent transition can be well explained using a new proposed theory--Energy gradient theory [1]. In this theory, the stability of a flow depends on the relative magnitude of energy gradient in streamwise direction and that in transverse direction, if there is no work input. In this note, it is shown based on the energy gradient theory that inviscid non-uniform flow is unstable if the energy in transverse direction is not constant. This new finding breaks the classical linear theory from Rayleigh that inviscid flow is unstable if the velocity profile has an inflection point in parallel flows and inviscid flow is stable if the velocity profile has no inflection point in parallel flow. Then, stability of rotating viscous and inviscid flows is studied, and two examples of rotating flows (rotating rigid body motion and free vortex motion) are shown, respectively.

Keywords: Viscous instability; Inviscid Instability; Rotating flows; Energy gradient; Energy loss; Non-uniform flow

PACS numbers:
47.20.-k Hydrodynamic stability
47.20.Gv Viscous instability
47.20.Ky Nonlinearity
47.15.Fe Stability of laminar flows
47.27.Cn Transition to turbulence
47.20.Ft Instability of shear flows

Stability of Rotating Viscous and Inviscid Flows

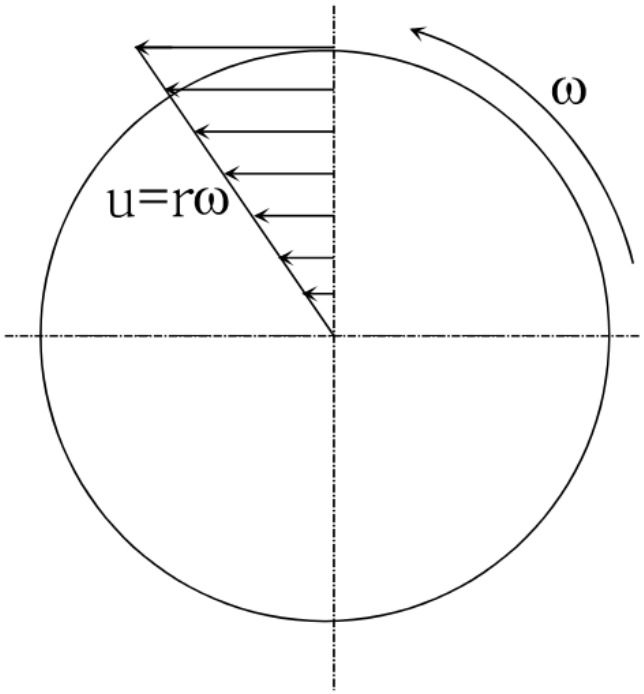

Fig. 3 Rigid body flow.

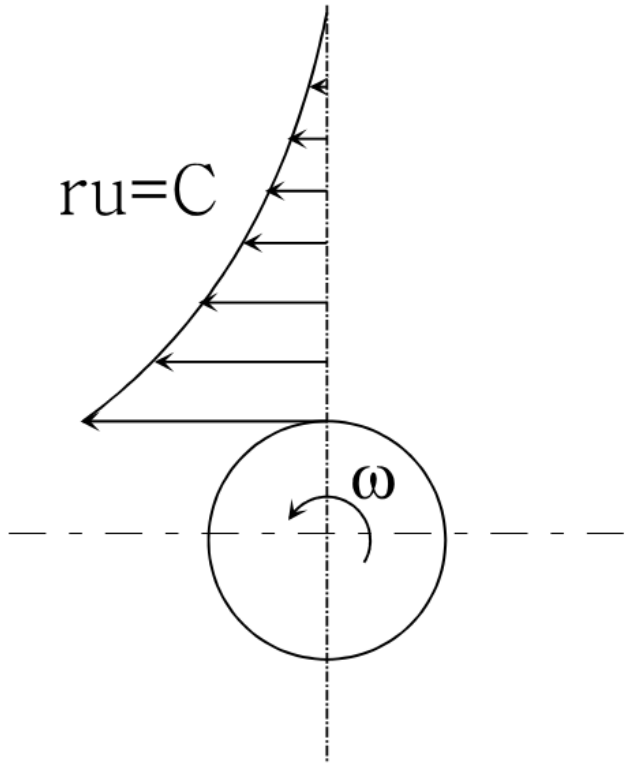

Fig. 4 Free vortex flow.

Long term Stability of vortex patches

Ann. scient. Éc. Norm. Sup.,
4e série, t. 26, 1993, p. 517 à 542.

PERSISTANCE DE STRUCTURES GÉOMÉTRIQUES DANS LES FLUIDES INCOMPRESSIBLES BIDIMENSIONNELS

PAR JEAN-YVES CHEMIN

RÉSUMÉ. – Dans cet article, on s'intéresse au comportement en temps grand d'une solution du système d'Euler relatif à un fluide parfait incompressible. On suppose que le tourbillon à l'instant initial est la fonction caractéristique d'un domaine borné régulier. Alors, pour tout temps, le tourbillon reste la fonction caractéristique d'un domaine borné ayant la même régularité.

ABSTRACT. – In this paper, we study the properties of a solution of the incompressible Euler system for large time. We suppose that the initial vorticity is the characteristic function of a regular bounded domain. Then the vorticity remains, for all time, the characteristic function of a bounded domain with the same regularity.

Mots-clefs : Champ de vecteurs (peu réguliers), régularité tangentielle, flot, tourbillon (poches de).

Introduction

Les résultats principaux exposés ici ont pour motivation première un problème classique de la mécanique d'un fluide parfait bidimensionnel : le problème des poches de tourbillon. Rappelons le cadre dans lequel nous allons travailler. Le mouvement d'un tel fluide est décrit par un champ de vecteurs sur le plan, dépendant du temps, noté $v(t, x)$ et vérifiant

$$(E)\quad \begin{cases} \partial_t v + v.\nabla v = -\nabla p \\ \operatorname{div} v = 0 \\ v_{|t=0} = v_0, \end{cases}$$

Jet In A Cross Flow (JICF)

High fidelity simulation and analysis of liquid jet atomization in a gaseous crossflow at intermediate Weber numbers

Xiaoyi Li and Marios C. Soteriou

Citation: Physics of Fluids **28**, 082101 (2016); doi: 10.1063/1.4959290
View online: http://dx.doi.org/10.1063/1.4959290
View Table of Contents: http://scitation.aip.org/content/aip/journal/pof2/28/8?ver=pdfcov
Published by the AIP Publishing

Jet In A Cross Flow (JICF): Grid strategies

additional coarsening via the introduction of Lagrangian droplets (to be referred as AMR-DRP) were also performed using 24 cores each. It is observed in Table III that, indeed, AMR and droplet transformation significantly reduce the grid-count and simulation cost. It is important to note that the 15.7 days UG computation using 5008 cores translates to at least 9 years if using 24 cores

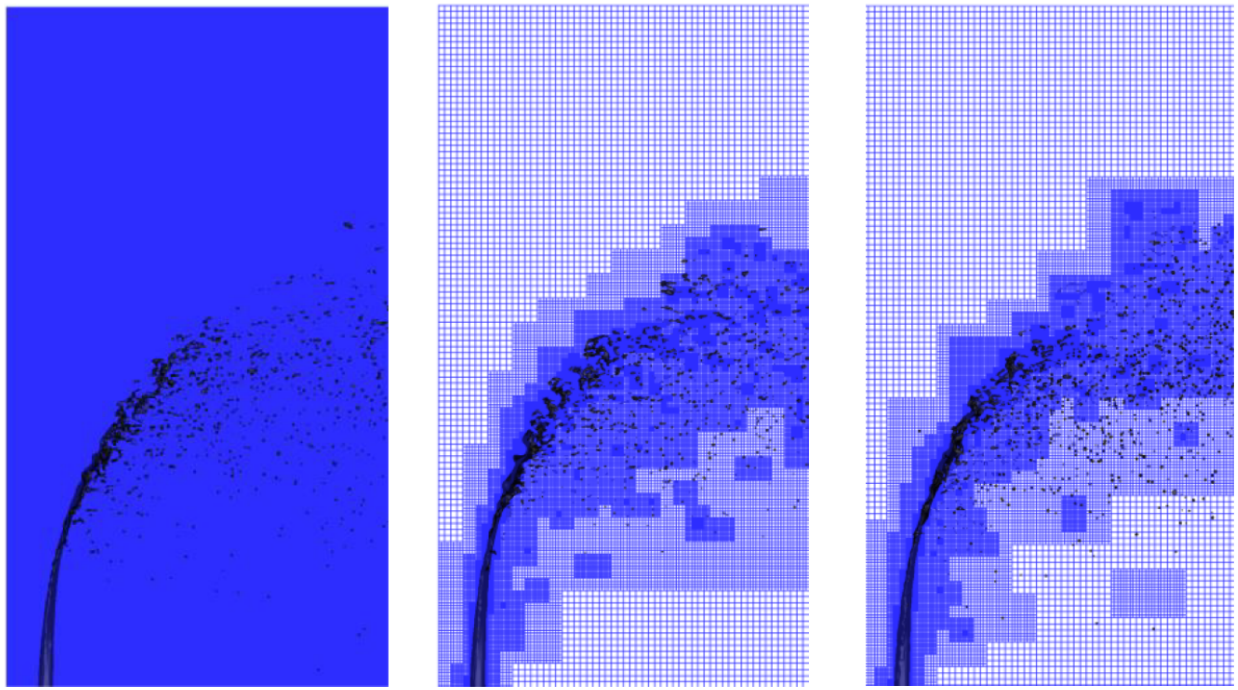

(a) (b) (c)

Jet In A Cross Flow (JICF): uniform grids versus AMR

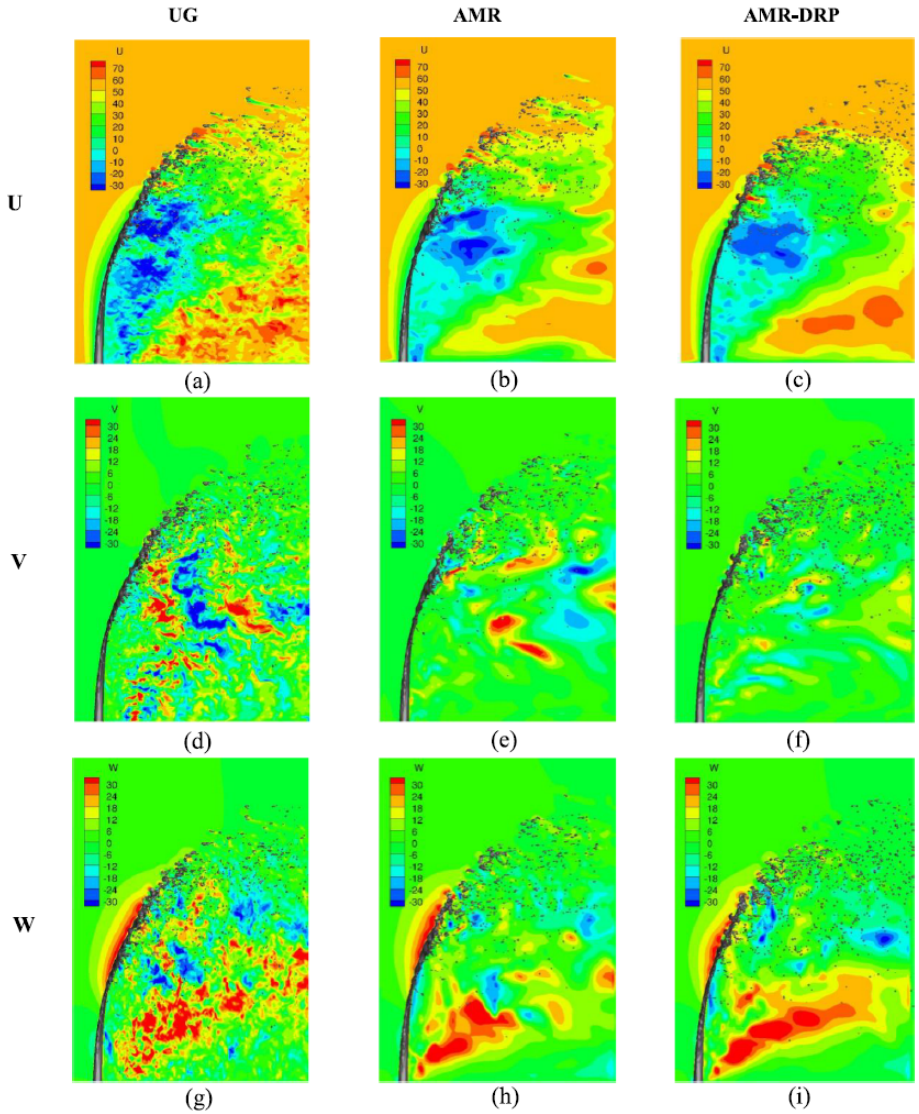

FIG. 5. Comparison of flow velocities at the mid-plane (y = 1 cm) using different grid configurations as in Fig. 2, We = 40.

Jet In A Cross Flow (JICF): patterns

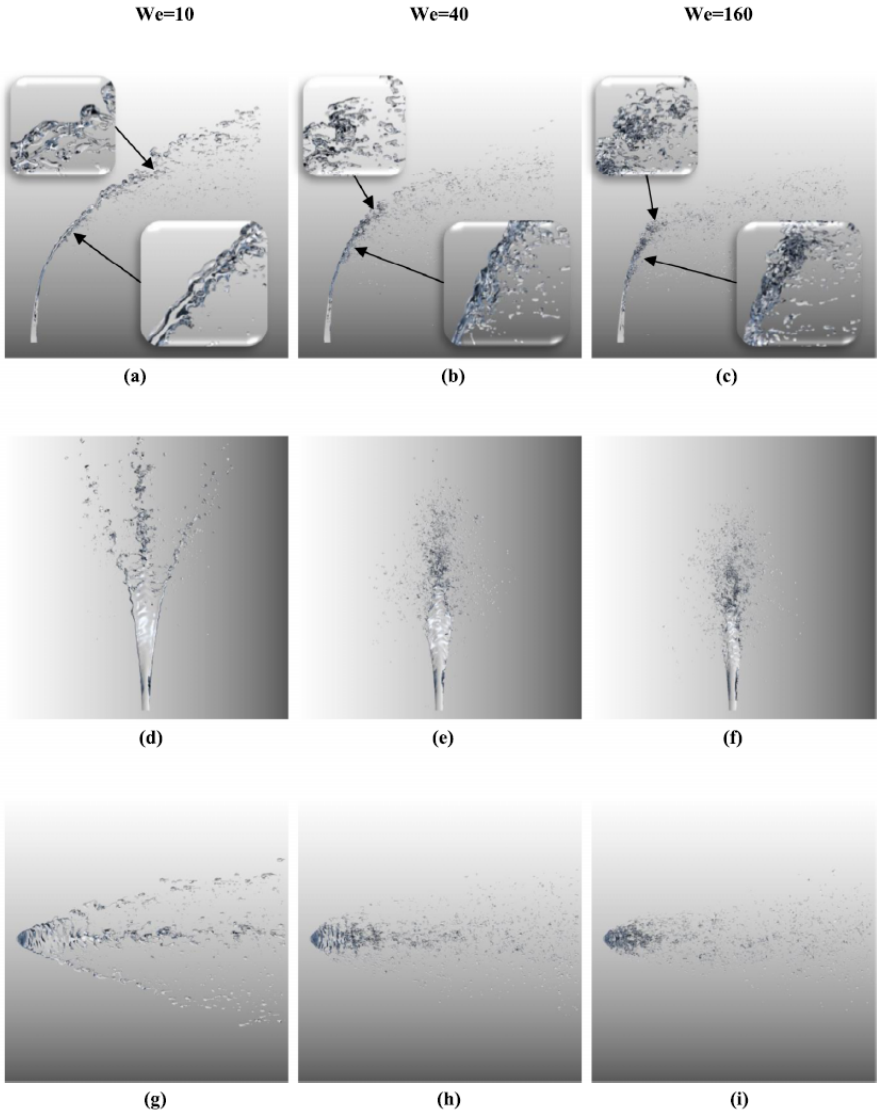

Further Motivations in multiphase flow

- Sea Spray (Dr. Doug Dommermuth, SUSTAIN tank in Miami)
- boiling in microgravity environments (Dr. Yongsheng Lian, Yang Liu)
- Laser assisted particle removal (Dr. M.Y. Hussaini, Dr. B. Unlusu, Dr. K. Lammers)
- spray in dishwashers (Dr. Yongsheng Lian)
- shock drop interaction (Dr. Yongsheng Lian)
- under water explosions (Weidlinger Assoc., Dr. Matt Jemison, Dr. Samet Kadioglu)
- Atomization and spray in diesel injectors (Dr. Marco Arienti, Cody Estebe, Dr. Yaohong Wang)
- Multiphase non-Newtonian flows (Dr. Mitsuhiro Ohta, Dr. Edwin Jimenez, Dr. Paul Stewart, Dr. Nathan Lay)

Paper that recently appeared online in Discrete and Continuous Dynamical Systems, Series B (AIMS)

doi: 10.3934/dcdsb.2017216

A space-time discontinuous Galerkin spectral element method for the Stefan problem

Chaoxu Pei, Mark Sussman and M. Yousuff Hussaini

Department of Mathematics, Florida State University, Tallahassee, FL, 32306, USA

A novel space-time discontinuous Galerkin (DG) spectral element method is presented to solve the one dimensional Stefan problem in an Eulerian coordinate system. This method employs the level set procedure to describe the time-evolving interface. To deal with the prior unknown interface, a backward transformation and a forward transformation are introduced in the space-time mesh. By combining an Eulerian description, i.e., a fixed frame of reference, with a Lagrangian description, i.e., a moving frame of reference, the issue of dealing with implicitly defined arbitrary shaped space-time elements is avoided. The *backward transformation* maps the unknown time-varying interface in the fixed frame of reference to a known stationary interface in the moving frame of reference. In the moving frame of reference, the transformed governing equations, written in the space-time framework, are discretized by a DG spectral element method in each space-time slab. The *forward transformation* is used to update the level set function and then to project the solution in each phase back from the moving frame of reference to the fixed Eulerian grid. Two options for calculating the interface velocity are presented, and both options exhibit spectral accuracy. Benchmark tests indicate that the method converges with spectral accuracy in both space and time for the temperature distribution and the interface velocity. A Picard iteration algorithm is introduced in order to solve the nonlinear algebraic system of equations and it is found that just a few iterations lead to convergence.

Keywords: Space-time, discontinuous Galerkin, spectral accuracy, transformations, the Stefan problem.

Mathematics Subject Classification: Primary: 65M70, 35R3.

Citation: Chaoxu Pei, Mark Sussman, M. Yousuff Hussaini. A space-time discontinuous Galerkin spectral element method for the Stefan problem. *Discrete & Continuous Dynamical Systems - B*, doi: 10.3934/dcdsb.2017216

Paper that recently appeared online in the International Journal of Computational Methods (2018)

International Journal of Computational Methods | Online Ready

No Access

A Space-Time Discontinuous Galerkin Spectral Element Method for Nonlinear Hyperbolic Problems

Chaoxu Pei, Mark Sussman and M. Yousuff Hussaini

https://doi.org/10.1142/S0219876218500937 | Cited by: 0

< Previous Next >

View Article Tools Share

Abstract

A space-time discontinuous Galerkin spectral element method is combined with two different approaches for treating problems with discontinuous solutions: (i) adding a space-time dependent artificial viscosity, and (ii) tracking the discontinuity with space-time spectral accuracy. A Picard iteration method is employed to solve nonlinear system of equations derived from the space-time DG spectral element discretization. Spectral accuracy in both space and time is demonstrated for the Burgers' equation with a smooth solution. For tests with discontinuities, the present space-time method enables better accuracy at capturing the shock strength in the element containing shock when higher order polynomials in both space and time are used. The spectral accuracy of the shock speed and location is demonstrated for the solution of the inviscid Burgers' equation obtained by the tracking method.

Preprint submitted to *International Journal of Computational Methods* December 21, 2017.

Keywords: Space-time · discontinuous Galerkin · spectral accuracy · shock capturing · shock tracking · picard iteration

Figures References Related Details

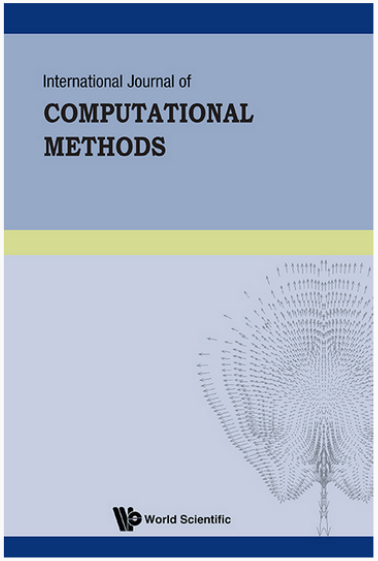

Online Ready

Metrics

Downloaded 4 times

History

Received 25 May 2017
Revised 21 December 2017
Accepted 10 January 2018

Published: 9 May 2018

Paper that recently appeared in "Online first" Journal of Scientific Computing

Journal of Scientific Computing
pp 1–34 | Cite as

New Multi-implicit Space–Time Spectral Element Methods for Advection–Diffusion–Reaction Problems

Authors | Authors and affiliations

Chaoxu Pei, Mark Sussman, M. Yousuff Hussaini

Article
First Online: 15 February 2018

77
Downloads

Abstract

Novel multi-implicit space–time spectral element methods are described for approximating solutions to advection–diffusion–reaction problems characterized by multiple time scales. The new methods are spectrally accurate in space and time and they are designed to be easy to implement and robust. In other words, given an existing stable low order operator split method for approximating solutions to PDEs exhibiting multiple scales, the algorithms described in this article enable one to easily extend a low order method to be a robust space–time spectrally accurate method. In space, two spectrally accurate advective flux reconstructions are proposed: extended element-wise flux reconstruction and non-extended element-wise flux reconstruction. In time, for the hyperbolic term(s), a low-order explicit I-stable building block time integration scheme is introduced in order to obtain a stable and efficient building block for the spectrally accurate space–time scheme. In this article, multiple spectrally accurate space discretization strategies, and multiple spectrally accurate time discretization strategies are compared to one another. It is found that all methods described are spectrally accurate with each method having distinguishing properties.

Keywords

Space–time | Operator splitting | Coupling strategy | Multiple time scales | Spectral accuracy

Other Related Work (single phase flow only)

- Zhang, "GePUP: Generic Projection and Unconstrained PPE for Fourth-Order Solutions of the Incompressible NavierStokes Equations with No-Slip Boundary Conditions" (2016)
- Kadioglu and Colak, "An essentially non-oscillatory spectral deferred correction method for conservation laws" (2016)
- Almgren, Aspden, Bell, Minion, "On the Use of Higher-Order Projection Methods for Incompressible Turbulent Flow" (2013)
- Fambri and Dumbser, "Spectral semi-implicit and space-time discontinuous Galerkin methods for the incompressible Navier-Stokes equations on staggered Cartesian grids" (2016)
- Morinishi, Lund, Vasilyev, Moin, "Fully conservative higher order finite difference schemes for incompressible flow" (JCP 1998)

Other Related Work continued

- Hu, Grossman, Steinhoff, "Numerical Method for Vorticity Confinement in Compressible Flow," AIAA Journal, 2002.
- Bauer, Cotter, "Energy-enstrophy conserving compatible finite element schemes for the rotating shallow water equations with slip boundary conditions," JCP 2018.
- Sidilkover, "Towards unification of the Vorticity Confinement and Shock Capturing (TVD and ENO/WENO) methods," JCP 2018.

Other Related Work continued (one of which is multiphase)

- Minion and Saye, "Higher-order temporal integration for the incompressible Navier-Stokes equations in bounded domains" (JCP 2018)
- Saye, "Implicit mesh discontinuous Galerkin methods and interfacial gauge methods for high-order accurate interface dynamics, with applications to surface tension dynamics, rigid body fluid-structure interaction, and free surface flow: Part I" (JCP 2017)
- Saye, "Interfacial gauge methods for incompressible fluid dynamics" (Science Advances 2016)

Navier-Stokes Equations for Multiphase flow

$$\boldsymbol{w}_t = \boldsymbol{F}_A[\boldsymbol{w}] + \boldsymbol{F}_D[\boldsymbol{w}] + \boldsymbol{F}_P[\boldsymbol{w}]$$

$$\phi_t^{(m)} + \boldsymbol{u} \cdot \nabla \phi^{(m)} = 0 \quad \text{Level set equations}$$

$$p = p^{(m)}(\rho, e) \quad (t, \boldsymbol{x}) \in \Omega^{(m)}, \text{compressible}$$

$$\nabla \cdot \boldsymbol{u} = 0 \quad (t, \boldsymbol{x}) \in \Omega^{(m)}, \text{incompressible}$$

$$\boldsymbol{w} = \begin{pmatrix} \rho \\ \rho \boldsymbol{u} \\ \rho E \end{pmatrix}$$

Navier-Stokes Equations for Multiphase flow (cont)

$$\boldsymbol{F}_A = -\nabla \cdot (\boldsymbol{u} \otimes \boldsymbol{w})$$

$$\boldsymbol{F}_D = \begin{pmatrix} 0 \\ \nabla \cdot \tau \\ \nabla \cdot (\boldsymbol{u} : \tau) - \nabla \cdot \boldsymbol{q} \end{pmatrix} \qquad \boldsymbol{F}_P = \begin{pmatrix} 0 \\ -\nabla p - \sigma\kappa(\phi)\nabla H \\ -\nabla \cdot (\boldsymbol{u}p) \end{pmatrix}$$

$$\boldsymbol{n} \cdot [-pI + \tau] \cdot \boldsymbol{n} = -\sigma\kappa(\phi) \qquad \boldsymbol{t} \cdot [-pI + \tau] \cdot \boldsymbol{n} = 0$$

Level Set Function

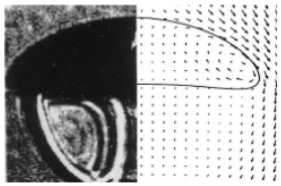

Figure 2 : Comparison of our numerical results with experimental results found in Hnat and Buckmaster (1976) where Re = 9.8, Mo = 0.065, and $C = 4.95$.

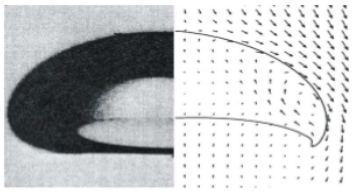

Figure 1 : Comparison of our numerical results with experimental results found in Bhaga and Weber (1981) where Eo = 243, Mo = 266, and Re = 7.77.

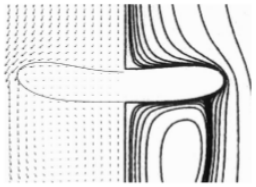

Figure 3 : Comparison of our numerical results with computational results found in Ryskin and Leal (1984) where Re = 100 and We = 10.

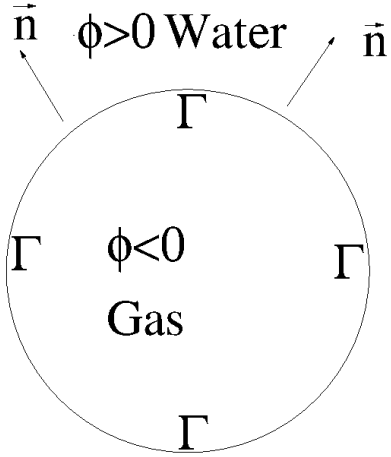

$$\Gamma = \{\boldsymbol{x} | \phi(t, \boldsymbol{x}) = 0\}$$

$$\boldsymbol{n} = \frac{\nabla \phi}{|\nabla \phi|} \qquad \kappa = \nabla \cdot \frac{\nabla \phi}{|\nabla \phi|}$$

Explicit Method

For example, an l-stable scheme:

$$\frac{\boldsymbol{w}^{n+1,(0)} - \boldsymbol{w}^{n}}{\Delta t} = \boldsymbol{F}_A[\boldsymbol{w}^n] + \boldsymbol{F}_D[\boldsymbol{w}^n] + \boldsymbol{F}_P[\boldsymbol{w}^n]$$

$$\frac{\boldsymbol{w}^{n+1} - \boldsymbol{w}^{n}}{\Delta t} = \boldsymbol{F}_A[\boldsymbol{w}^{n+1,(0)}] + \boldsymbol{F}_D[\boldsymbol{w}^{n+1,(0)}] + \boldsymbol{F}_P[\boldsymbol{w}^{n+1,(0)}]$$

Bao and Jin, 2001, 2003
Nourgaliev and Theofanous, 2007

Implicit (Monolithic) Method

e.g. Crank-Nicholson method:

$$\frac{\boldsymbol{w}^{n+1} - \boldsymbol{w}^{n}}{\Delta t} = \frac{\boldsymbol{F}_A[\boldsymbol{w}^{n}] + \boldsymbol{F}_A[\boldsymbol{w}^{n+1}]}{2} + \frac{\boldsymbol{F}_D[\boldsymbol{w}^{n}] + \boldsymbol{F}_D[\boldsymbol{w}^{n+1}]}{2} + \frac{\boldsymbol{F}_P[\boldsymbol{w}^{n}] + \boldsymbol{F}_P[\boldsymbol{w}^{n+1}]}{2}$$

Rasetarinara and Hussaini, 2001
Roberts, Sidilkover, Tsynkov, 2002

Divide and Conquer (operator split) Method

$$\frac{\boldsymbol{w}^{n+1,(0)} - \boldsymbol{w}^{n}}{\Delta t} = \boldsymbol{F}_A[\boldsymbol{w}^{n}]$$

$$\frac{\boldsymbol{w}^{n+1,(1)} - \boldsymbol{w}^{n}}{\Delta t} = \boldsymbol{F}_A[\boldsymbol{w}^{n+1,(0)}]$$

$$\frac{\boldsymbol{w}^{n+1,(2)} - \boldsymbol{w}^{n+1,(1)}}{\Delta t} = \boldsymbol{F}_D[\boldsymbol{w}^{n+1,(2)}]$$

$$\frac{\boldsymbol{w}^{n+1} - \boldsymbol{w}^{n+1,(2)}}{\Delta t} = \boldsymbol{F}_P[\boldsymbol{w}^{n+1}]$$

Douglas and Rachford, 1956
Speth, Green, MacNamara, Strang, 2013
Kwatra, Su, Gretarsson, Fedkiw, 2009
Jemison, Sussman, Arienti, 2014
Bell, Colella, Glaz, 1989

Spectral Deferred Correction Method

Spectral in time

Processes with disparate temporal scales are treated independently, but coupled iteratively by a series of the deferred correction procedure.

Bourlioux, Layton, Minion, 2003
Layton, Minion, 2004
Kadioglu, 2016
Pei, Sussman, Hussaini, 2018
Minion and Saye, 2018

The space time slab

All variables are discretized at the Legendre Gauss Lobatto points with respect to time.

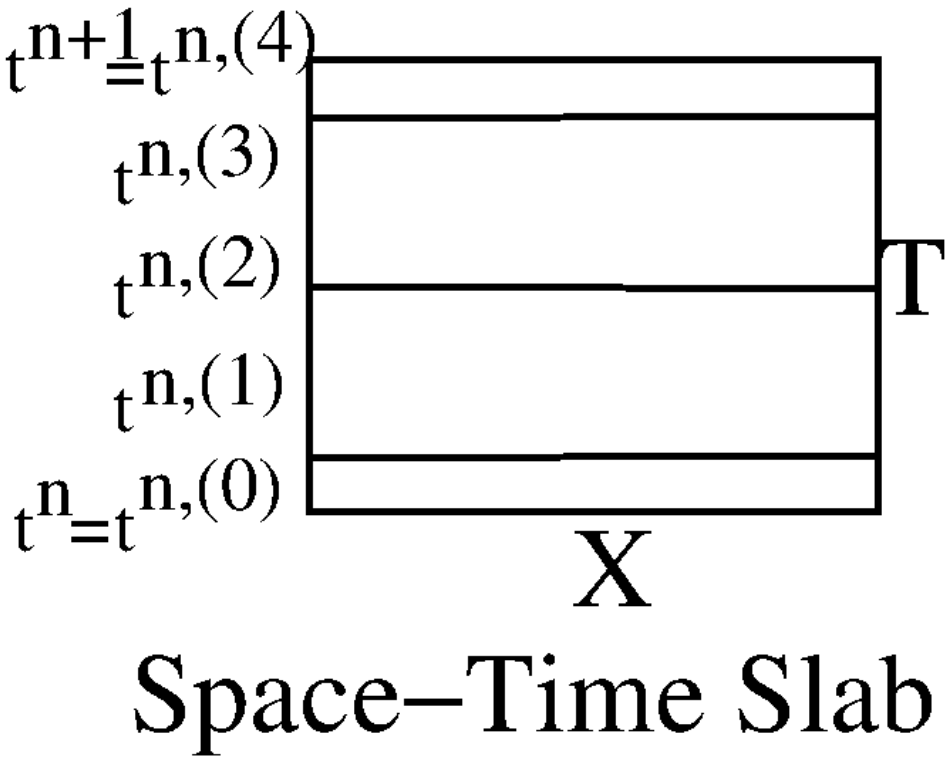

Coupling strategy 1

for $k = 0, \ldots, r$, for $m = 0, \ldots, r$,

$$w_A^{n,(m+1),k+1} = w^{n,(m),k+1} + \int_{t^{n,(m)}}^{t^{n,(m+1)}} [F_A(w_A^{k+1}) - F_A(w_A^k)]d\tau + \int_{t^{n,(m)}}^{t^{n,(m+1)}} [F_A(w^k)]d\tau,$$

$$w_{AD}^{n,(m+1),k+1} = w_A^{n,(m+1),k+1} + \int_{t^{n,(m)}}^{t^{n,(m+1)}} [F_D(w_{AD}^{k+1}) - F_D(w_{AD}^k)]d\tau + \int_{t^{n,(m)}}^{t^{n,(m+1)}} [F_D(w^k)]d\tau,$$

$$w^{n,(m+1),k+1} = w_{AD}^{n,(m+1),k+1} + \int_{t^{n,(m)}}^{t^{n,(m+1)}} [F_P(w^{k+1}) - F_P(w^k)]d\tau + \int_{t^{n,(m)}}^{t^{n,(m+1)}} [F_P(w^k)]d\tau.$$

The second integral is evaluated with a higher-order quadrature rule, i.e., Gauss quadrature, while the first integral is discretized by a low-order time integration scheme, i.e., first order time integration scheme.

Coupling strategy 2

for $k = 0, \ldots, r$, for $m = 0, \ldots, r$,

$$w_A^{n,(m+1),k+1} = w^{n,(m),k+1} + \int_{t^{n,(m)}}^{t^{n,(m+1)}} [F_A(w_A^{k+1}) - F_A(w_A^k)]d\tau + \int_{t^{n,(m)}}^{t^{n,(m+1)}} [F_A(w^k)]d\tau,$$

$$w_{ADP}^{n,(m+1),k+1} = w_A^{n,(m+1),k+1} + \int_{t^{n,(m)}}^{t^{n,(m+1)}} [F_D(w_{ADP}^{k+1}) - F_D(w^k)]d\tau + \int_{t^{n,(m)}}^{t^{n,(m+1)}} [F_D(w^k) + F_P(w^k)]d\tau,$$

$$w^{n,(m+1),k+1} = w_{ADP}^{n,(m+1),k+1} + \int_{t^{n,(m)}}^{t^{n,(m+1)}} [F_P(w^{k+1}) - F_P(w^k)]d\tau.$$

Example building blocks for the Advection-diffusion-reaction equation

To describe the multi implicit space-time spectral element method, we take the following advection-diffusion-reaction equation as an example,

$$
\begin{aligned}
&w_t + \nabla \cdot (\mathbf{u}w) = \nu \mathbf{\Delta} \mathbf{w} + \lambda \mathbf{w}, \quad \mathbf{x} \in \mathbf{\Omega} \\
&w(\mathbf{x}, \mathbf{0}) = \mathbf{w_0}, \\
&w|_{\partial\Omega} = g,
\end{aligned}
$$

where $\mathbf{u} = (\mathbf{u}, \mathbf{v})^\top$ is velocity vector, ν and λ are constant.

Both diffusion and reaction processes are on faster time scales compared to advection process.

Discretization in time

After applying spectral element discretizations in space (details will soon follow), we obtain a system of ODEs as follows,

$$\frac{\partial w}{\partial t} = F_A(w) + F_D(w) + F_R(w),$$

where

- $F_A(w)$ denotes the spatial discretization of advection term $\nabla \cdot (\mathbf{uw})$.
- $F_D(w)$ denotes the spatial discretization of diffusion term $\nu \Delta w$). (Stiff term.)
- $F_R(w)$ denotes the spatial discretization of reaction term $f_r(w)$. (Stiff term.)

Low order building blocks

In order to avoid stringent time step, we use an implicit treatment for both diffusion and reaction processes while an explicit l-scheme time integration scheme for the advection process.

l-scheme building block for advection

$$\frac{\boldsymbol{w}^{n+1,(0)} - \boldsymbol{w}^{n}}{\Delta t} = \boldsymbol{F}_A[\boldsymbol{w}^{n}]$$

$$\frac{\boldsymbol{w}^{n+1} - \boldsymbol{w}^{n}}{\Delta t} = \boldsymbol{F}_A[\boldsymbol{w}^{n+1,(0)}]$$

A comparison of stability region between forward Euler scheme and l-stable scheme for advection:

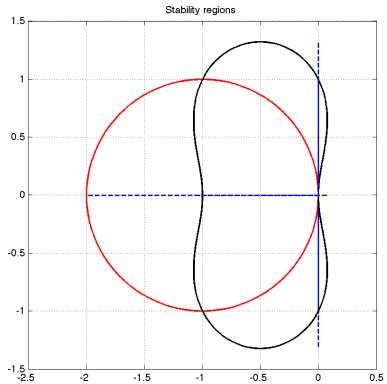

Ref: Bao and Jin, 2001, 2003.

Backwards Euler building blocks for diffusion and reaction

$$\frac{\boldsymbol{w}^{n+1} - \boldsymbol{w}^{n}}{\Delta t} = \boldsymbol{F}_D[\boldsymbol{w}^{n+1}]$$

$$\frac{\boldsymbol{w}^{n+1} - \boldsymbol{w}^{n}}{\Delta t} = \boldsymbol{F}_R[\boldsymbol{w}^{n+1}]$$

The spectral element grid

Pressure, Density, Temperature, and Level set function are located at the tensor product Legendre Gauss points with respect to the space coordinates. The velocity is located at the staggared Gauss Lobatto and Gauss points with respect to the space points.

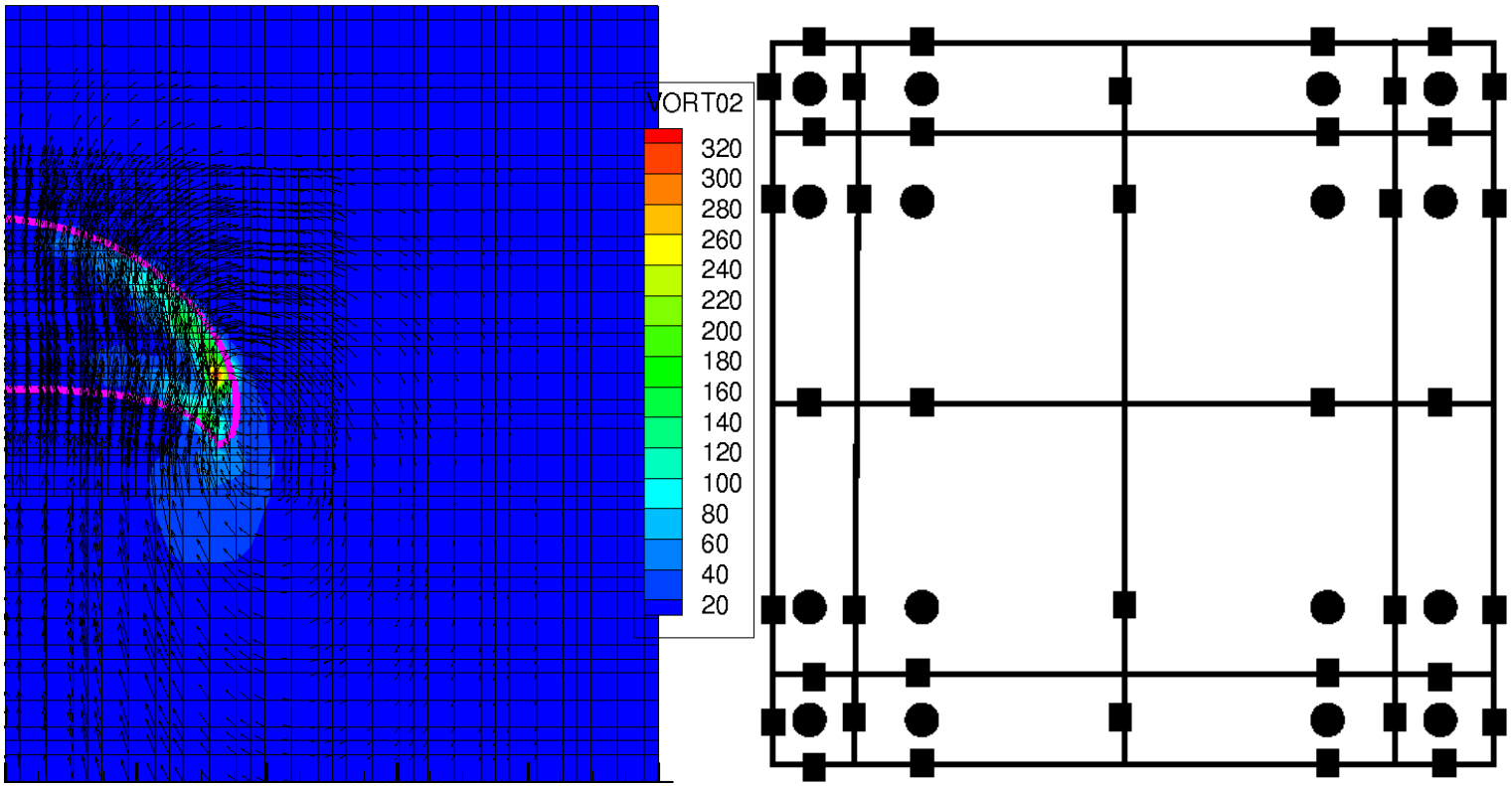

The piecewise spectral element grid

Pressure, Density, Temperature, and Level set function are located at the tensor product Legendre Gauss points with respect to the space coordinates. The velocity is located at the staggared Gauss Lobatto and Gauss points with respect to the space points. Each mixed element and one surrounding element are discretized using a standard piecewise continuous finite volume method.

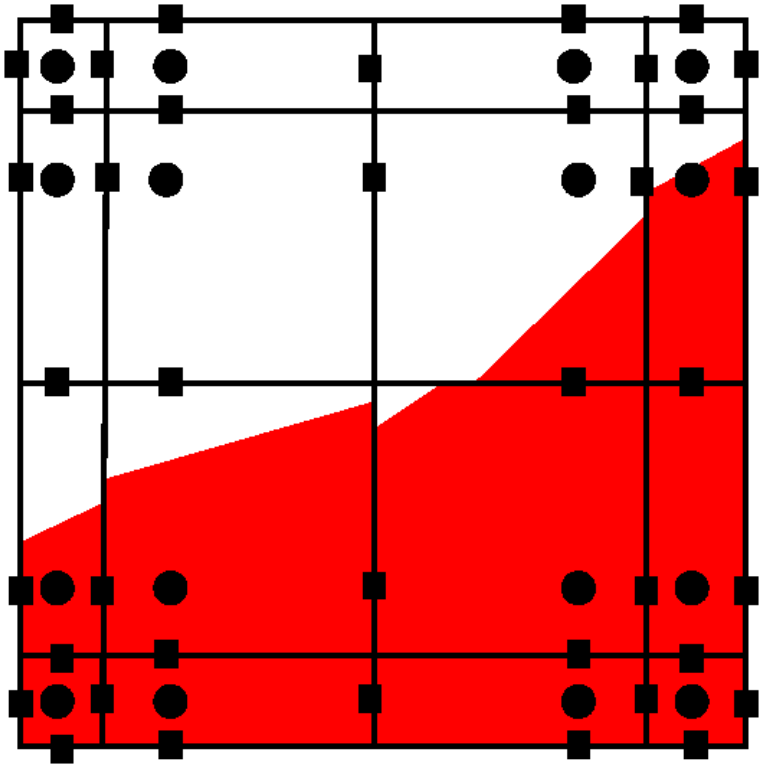

Discretization at a coarse-fine interface

Prolongation and restriction are approximated using high order Lagrange interpolating polynomials (no Runge Phenomenon). For the multigrid preconditioner though, only second order Prolongation or Restriction algorithms are used.

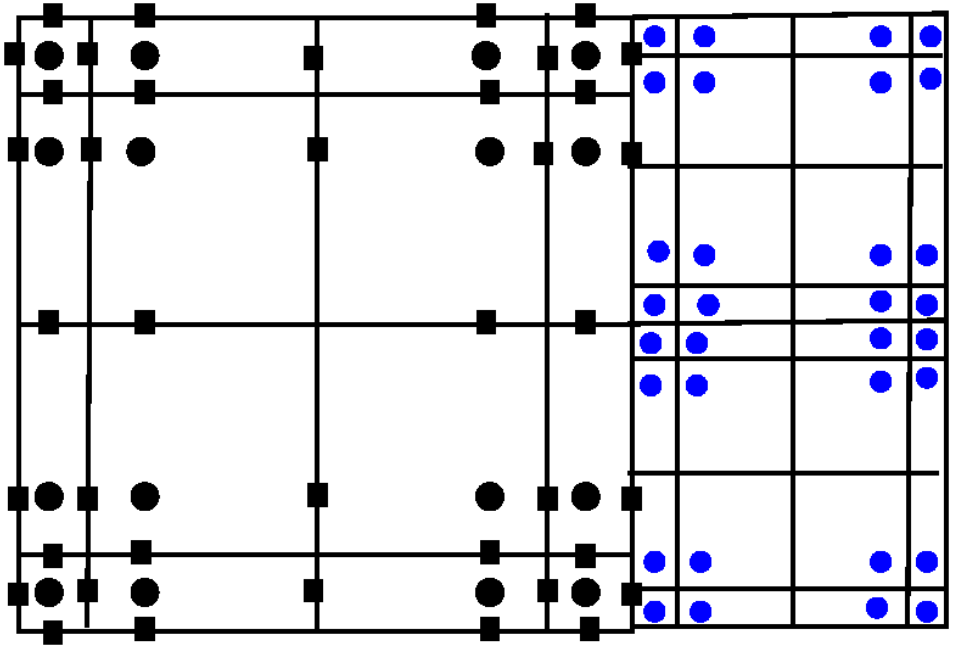

Spectrally Accurate and Conservative Discretization in Space

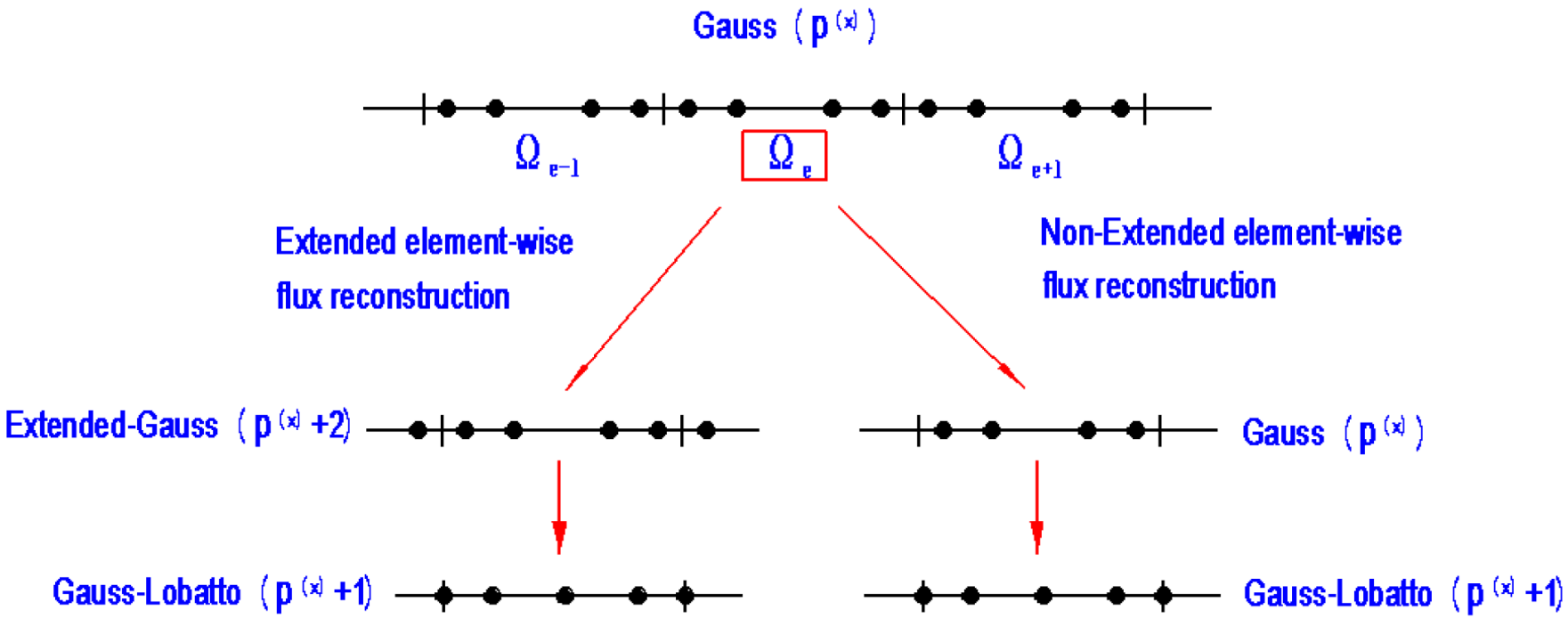

Advection fluxes: interpolate from Extended-Gauss grid to Gauss-Lobatto grid.
Diffusive fluxes: find derivative of Extended-Gauss grid interpolant at the Gauss-Lobato grid points.

Spectrally Accurate and Conservative Discretization in Space: near a boundary

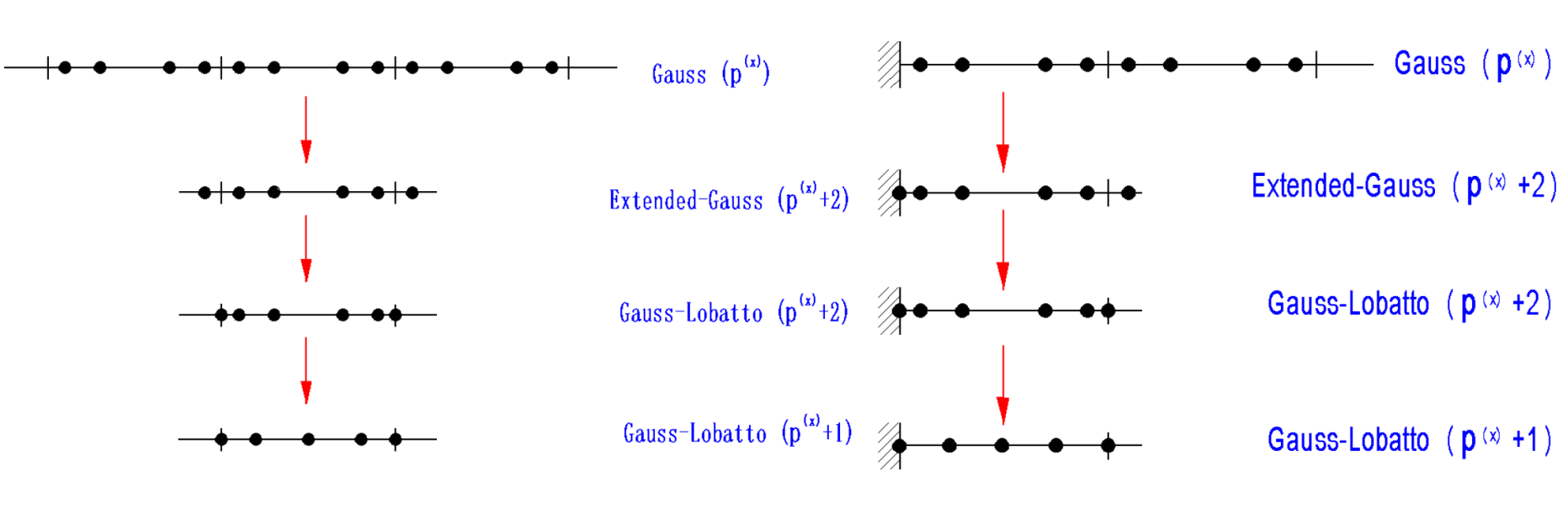

Gauss Legendre vs Gauss Chebychev?

The error for polynomial interpolation is:

$$f(x) = P_n(x) + R_n(x)$$

$$R_n(x) = \frac{f^{(n+1)}(\xi(x))}{(n+1)!}\Pi_{j=0}^{n}(x - x_j)$$

On the one hand, Gauss Chebychev polynomial interpolation optimizes the part of $R_n(x)$ corresponding to $\Pi_{j=0}^{n}(x - x_j)$. On the other hand, Gauss Legendre polynomial interpolation optimizes the degree of precision for numerical quadrature. We have found, experimentally, that Gauss Chebychev placement of discrete points is unstable. A recent article that might shed light on this issue: Gassner, Gregor J., Andrew R. Winters, and David A. Kopriva. "Split form nodal discontinuous Galerkin schemes with summation-by-parts property for the compressible Euler equations." Journal of Computational Physics 327 (2016): 39-66.

Numerical tests: Advection-diffusion-reaction equation

$$
\begin{aligned}
&w_t + \nabla \cdot (\mathbf{u}\mathbf{w}) = \nu \boldsymbol{\Delta} \mathbf{w} + \lambda \mathbf{w}, \quad \mathbf{x} \in \boldsymbol{\Omega} \\
&w(\mathbf{x}, \mathbf{0}) = \mathbf{w_0}, \\
&w|_{\partial\Omega} = g,
\end{aligned}
$$

where $\mathbf{u} = (\mathbf{u}, \mathbf{v})^\top$ is velocity vector, ν and λ are constant.

Both diffusion and reaction processes are on faster time scales compared to advection process.

Numerical tests

On a computational domain $\Omega = [0,1] \times [0,1]$, we solve a advection-diffusion-reaction problem with periodic boundary conditions. The velocity vector $\mathbf{u} = (\mathbf{u}, \mathbf{v})^\top$ is set to be $(1,1)^\top$, and $\nu = 0.04$ and $\lambda = 5.0$.

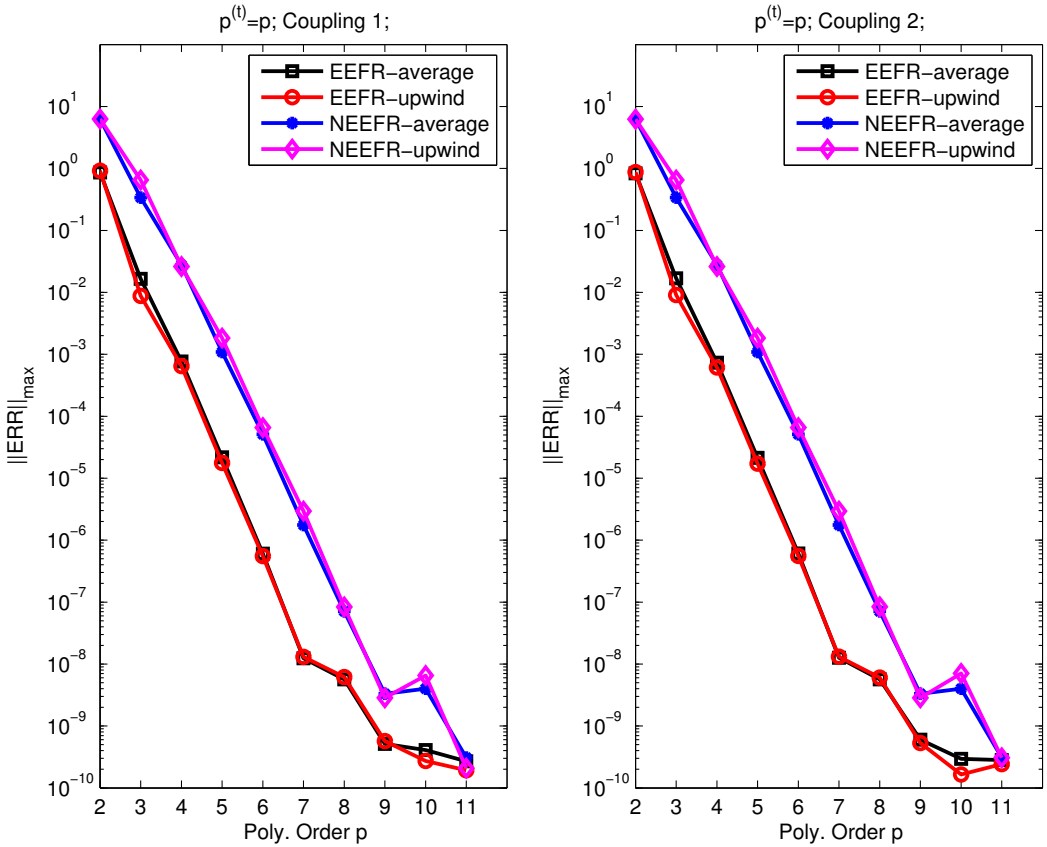

Figure: Errors in the solution as a function of polynomial order in space p in a semi-log plot. The simulation is computed up to 1.0 with 5×5 spatial tessellation and $E^{(t)} = 80$.

Overall order of accuracy

Overall order of convergence			
$(p^{(x)}, p^{(y)})$, $(p^{(t)}, K)$	$(E^{(x)} \times E^{(y)}, E^{(t)})$	Coupling 1	Coupling 2
(4, 4), (4, 4)	$(5 \times 5, 80)$	—	—
	$(10 \times 10, 160)$	5.1	5.2
	$(20 \times 20, 320)$	4.4	4.4
(4, 4), (4, 5)	$(5 \times 5, 40)$	—	—
	$(10 \times 10, 80)$	5.3	5.7
	$(20 \times 20, 160)$	5.0	5.1
(5, 5), (5, 5)	$(5 \times 5, 80)$	—	—
	$(10 \times 10, 160)$	5.7	5.7
	$(20 \times 20, 320)$	5.6	5.6
(5, 5), (5, 6)	$(5 \times 5, 40)$	—	—
	$(10 \times 10, 80)$	6.0	6.0
	$(20 \times 20, 160)$	5.8	5.8

Either reduce the time step or increase the number of iterations per step can achieve $\min\{p^{(x)}+1, p^{(y)}+1, p^{(t)}+1, K\}$, where K is the number of iterations per time step.

Order of accuracy in space

Order of convergence in space			
$(p^{(x)}, p^{(y)}), (p^{(t)}, K)$	$(E^{(x)} \times E^{(y)}, E^{(t)})$	Coupling 1	Coupling 2
(4, 4), (6, 8)	$(3 \times 3, 100)$	—	—
	$(6 \times 6, 100)$	5.7	5.7
	$(12 \times 12, 100)$	6.0	6.0
(5,5) ,(6,8)	$(3 \times 3, 100)$	—	—
	$(6 \times 6, 100)$	6.5	6.5
	$(12 \times 12, 100)$	5.7	5.7
(6,6), (6, 8)	$(3 \times 3, 100)$	—	—
	$(6 \times 6, 100)$	8.1	8.1
	$(12 \times 12, 100)$	8.1	8.1
(7,7), (6, 8)	$(3 \times 3, 100)$	—	—
	$(6 \times 6, 100)$	8.2	8.2
	$(12 \times 12, 100)$	8.2	8.5

Order of accuracy in time

Order of convergence in time			
$(p^{(x)}, p^{(y)})$, $(p^{(t)}, K)$	$(E^{(x)} \times E^{(y)}, E^{(t)})$	Coupling 1	Coupling 2
(8, 8), (4, 5)	$(5 \times 5, 40)$	—	—
	$(5 \times 5, 80)$	5.0	5.0
	$(5 \times 5, 160)$	5.0	5.0
(8, 8), (5, 5)	$(5 \times 5, 40)$	—	—
	$(5 \times 5, 80)$	4.9	4.9
	$(5 \times 5, 160)$	5.0	5.0
(8, 8), (4, 6)	$(5 \times 5, 40)$	—	—
	$(5 \times 5, 80)$	6.1	6.2
	$(5 \times 5, 160)$	5.8	5.7
(9, 9), (5, 6)	$(5 \times 5, 40)$	—	—
	$(5 \times 5, 80)$	6.1	6.1
	$(5 \times 5, 160)$	6.0	6.0
(9, 9), (6, 6)	$(5 \times 5, 40)$	—	—
	$(5 \times 5, 80)$	6.0	6.0
	$(5 \times 5, 160)$	5.9	5.9

Outline of hierarchical method

1. Advection: CISL-MOF in "low order" regions, Free-stream preserving l-scheme building block otherwise.
2. Diffusion: Backwards Euler building block: Multigrid preconditioned BiCGStab.
3. Compressible or Incompressible Projection method: Multigrid preconditioned BiCGStab.
4. After regridding: A spectrally accurate "projection" guarantees that the value of $\nabla \cdot \boldsymbol{U}$ is preserved.
5. "BoxLib" with tiling: an adaptive mesh refinement software framework.

"BoxLib" also now known as "AMReX"

SIAM J. SCI. COMPUT.
Vol. 38, No. 5, pp. S156–S172

BOXLIB WITH TILING: AN ADAPTIVE MESH REFINEMENT SOFTWARE FRAMEWORK*

WEIQUN ZHANG†, ANN ALMGREN†, MARCUS DAY†, TAN NGUYEN‡, JOHN SHALF§, AND DIDEM UNAT¶

Abstract. In this paper we introduce a block-structured adaptive mesh refinement software framework that incorporates tiling, a well-known loop transformation. Because the multiscale, multiphysics codes built in BoxLib are designed to solve complex systems at high resolution, performance on current and next generation architectures is essential. With the expectation of many more cores per node on next generation architectures, the ability to effectively utilize threads within a node is essential, and the current model for parallelization will not be sufficient. We describe a new version of BoxLib in which the tiling constructs are embedded so that BoxLib-based applications can easily realize expected performance gains without extra effort on the part of the application developer. We also discuss a path forward to enable future versions of BoxLib to take advantage of NUMA-aware optimizations using the TiDA portable library.

Key words. high-performance computing, software framework, tiling

AMS subject classification. 97N80

DOI. 10.1137/15M102616X

Properly Nested grids

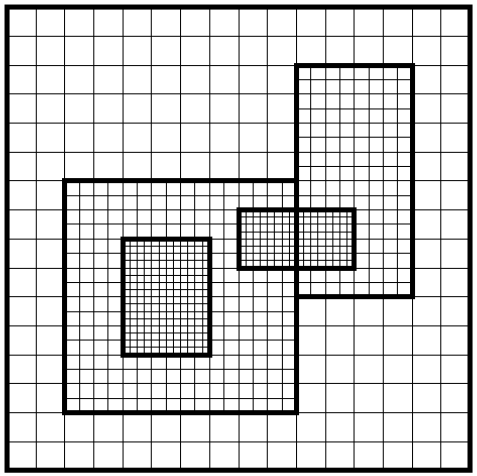

FIG. 2. *Cartoon of AMR grids with two levels of factor* 2 *refinement. The coarsest grid covers the domain with* 16^2 *cells. Bold lines represent grid boundaries. The two intermediate resolution grids are at level* 1 *and the cells are a factor of 2 finer than those at level* 0*. The two finest grids are at level* 2 *and the cells are a factor of 2 finer than the level* 1 *cells. Note that there is no direct parent-child connection. The data for each grid are contained in an object called FArrayBox (see section* 3.1*). In this example, there are* 1*,* 2*, and* 2 *FArrayBox objects on levels* 0*,* 1*, and* 2*, respectively. FArrayBox objects on each level are organized into an object called MultiFab (Multiple FArrayBox).*

Tiling

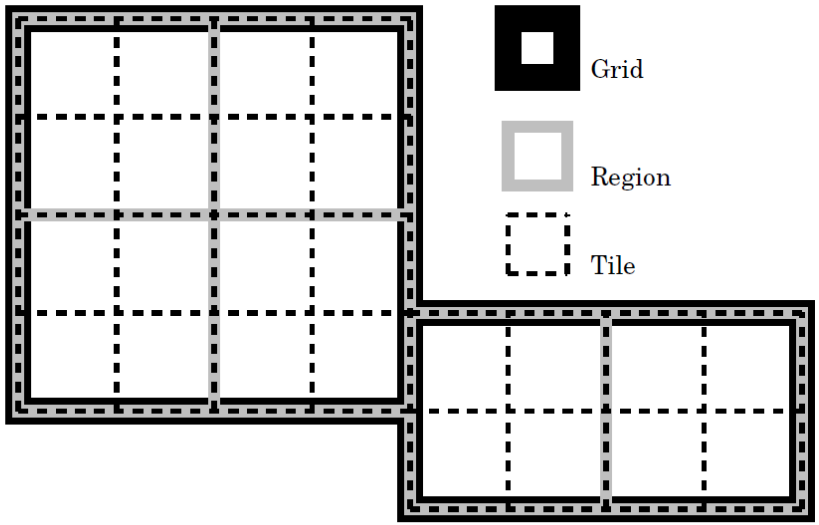

FIG. 1. *Grid, region, and tile. In this example of regional tiling, there are two grids. The grid on the left contains four regions, and the grid on the right contains two regions. Each region is split into four logical tiles in iteration space. The floating point data are allocated contiguously in each region; thus the data within a grid are not in one contiguous block. Note that logical tiles do not affect the data layout in memory.*

Single fluid, Inviscid, Incompressible Flow tests

$$\boldsymbol{u}_t + \boldsymbol{u} \cdot \nabla \boldsymbol{u} = -\nabla p \quad \nabla \cdot \boldsymbol{u} = 0$$

$$\boldsymbol{u}_t = -\boldsymbol{u} \cdot \nabla \boldsymbol{u} - \nabla p \equiv F_A(w) + F_P(w) \quad \nabla \cdot \boldsymbol{u} = 0$$

$$w = (\boldsymbol{u}, p)$$

Low order I scheme building block for advection

$$\frac{\boldsymbol{w}^{n+1,(0)} - \boldsymbol{w}^{n}}{\Delta t} = \boldsymbol{F}_A[\boldsymbol{w}^{n}]$$

$$\frac{\boldsymbol{w}^{n+1} - \boldsymbol{w}^{n}}{\Delta t} = \boldsymbol{F}_A[\boldsymbol{w}^{n+1,(0)}]$$

Projection method for the pressure gradient building block

$$\frac{\boldsymbol{u}^{n+1} - \boldsymbol{u}^*}{\Delta t} = -\nabla p^{n+1} \quad \nabla \cdot \boldsymbol{u}^{n+1} = 0$$

$$\nabla \cdot \left(\frac{\boldsymbol{u}^{n+1} - \boldsymbol{u}^*}{\Delta t} = -\nabla p^{n+1} \right)$$

$$\Delta p^{n+1} = \frac{\nabla \cdot \boldsymbol{u}^*}{\Delta t}$$

$$\boldsymbol{u}^{n+1} = \left(I - \nabla \Delta^{-1} \nabla \cdot \right) \boldsymbol{u}^*$$

smooth test problem

At $t = 0$,

$$u = -\sin(2\pi x)\cos(2\pi y) + u_0$$

$$v = \cos(2\pi x)\sin(2\pi y) + v_0$$

Periodic boundary conditions, the following quantities should be constant with respect to time:

$$\int \boldsymbol{u} \cdot \boldsymbol{u}/2 dx \qquad \text{Kinetic Energy}$$

$$\int \boldsymbol{w} \cdot \boldsymbol{w} dx \quad \boldsymbol{w} = \nabla \times \boldsymbol{u} \qquad \text{Enstrophy}$$

smooth problem, contours of the initial vorticity magnitude

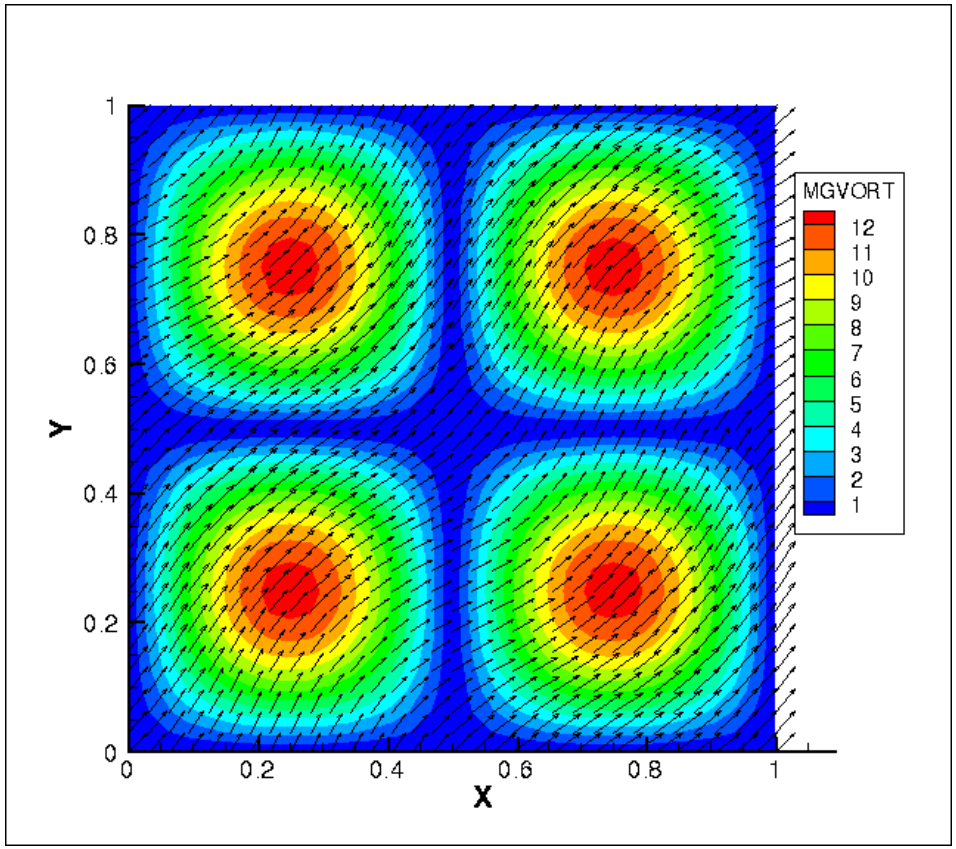

smooth problem, plot of $||w - w^{exact}||_\infty$ versus time

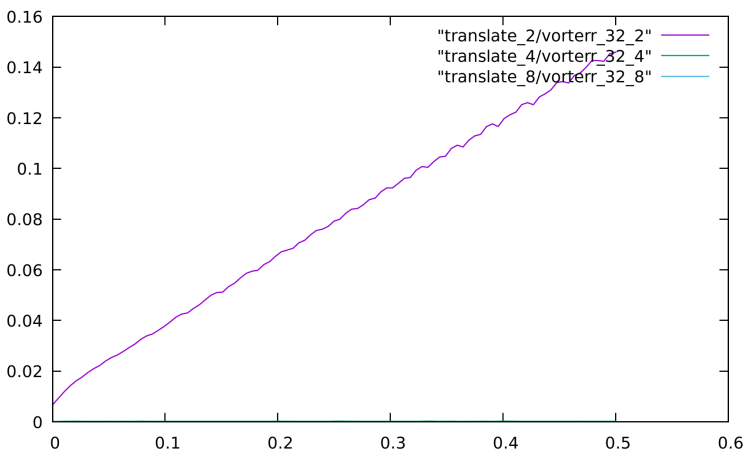

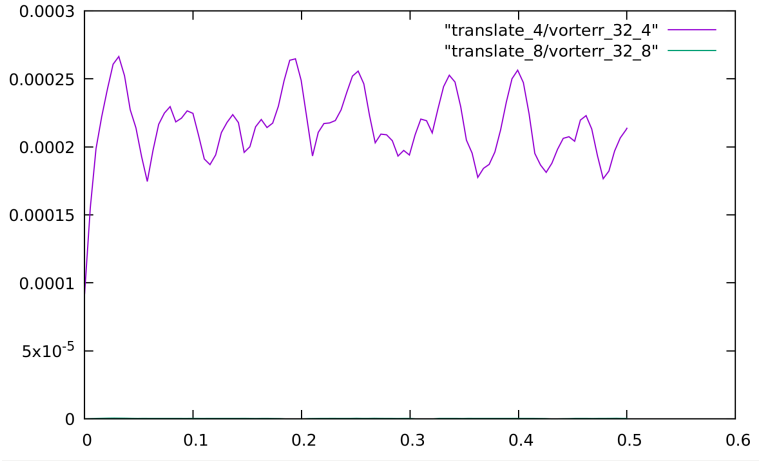

smooth problem with AMR patch, plot of $||w - w^{exact}||_\infty$ versus time

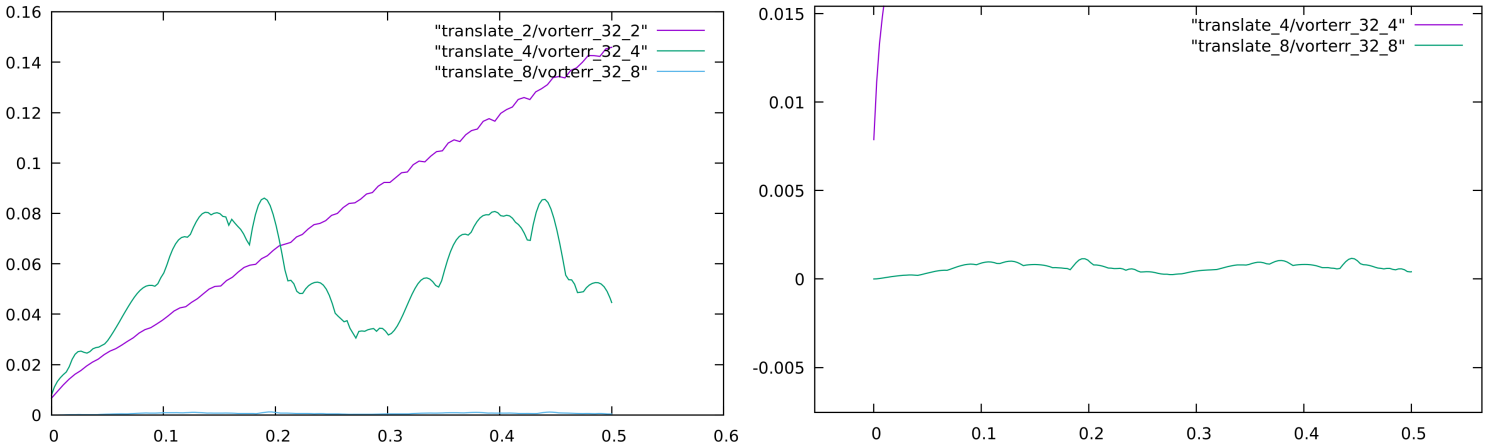

Double shear layer

(Bell, Colella, Glaz, JCP) At $t = 0$,

$$u = \tanh(30(y - 1/4)) \quad y \leq 1/2$$
$$u = \tanh(30(3/4 - y)) \quad y > 1/2$$

$$v = \sin(2\pi x)/20$$

Periodic boundary conditions, the following quantities should be constant with respect to time:

$$\int \boldsymbol{u} \cdot \boldsymbol{u}/2 dx \qquad \text{Kinetic Energy}$$

$$\int \boldsymbol{w} \cdot \boldsymbol{w} dx \quad \boldsymbol{w} = \nabla \times \boldsymbol{u} \qquad \text{Enstrophy}$$

Double shear layer 8th order 256x256

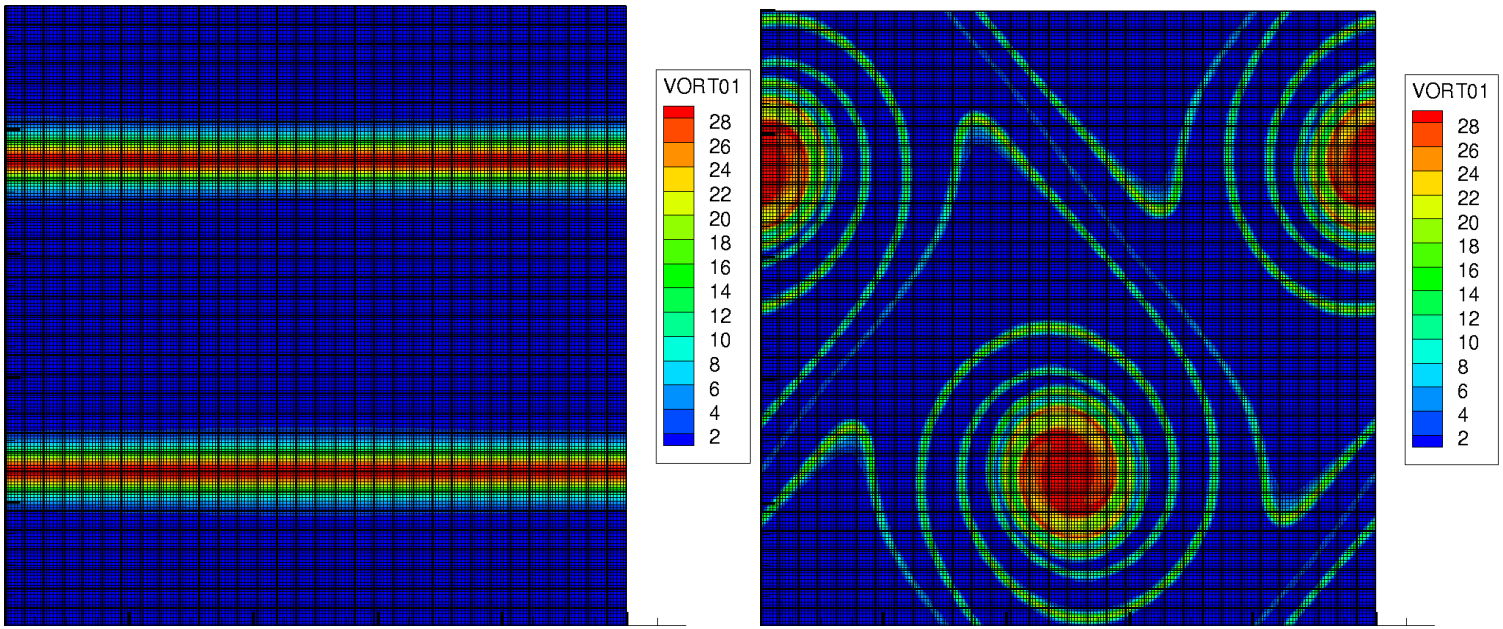

Enstrophy Double shear layer

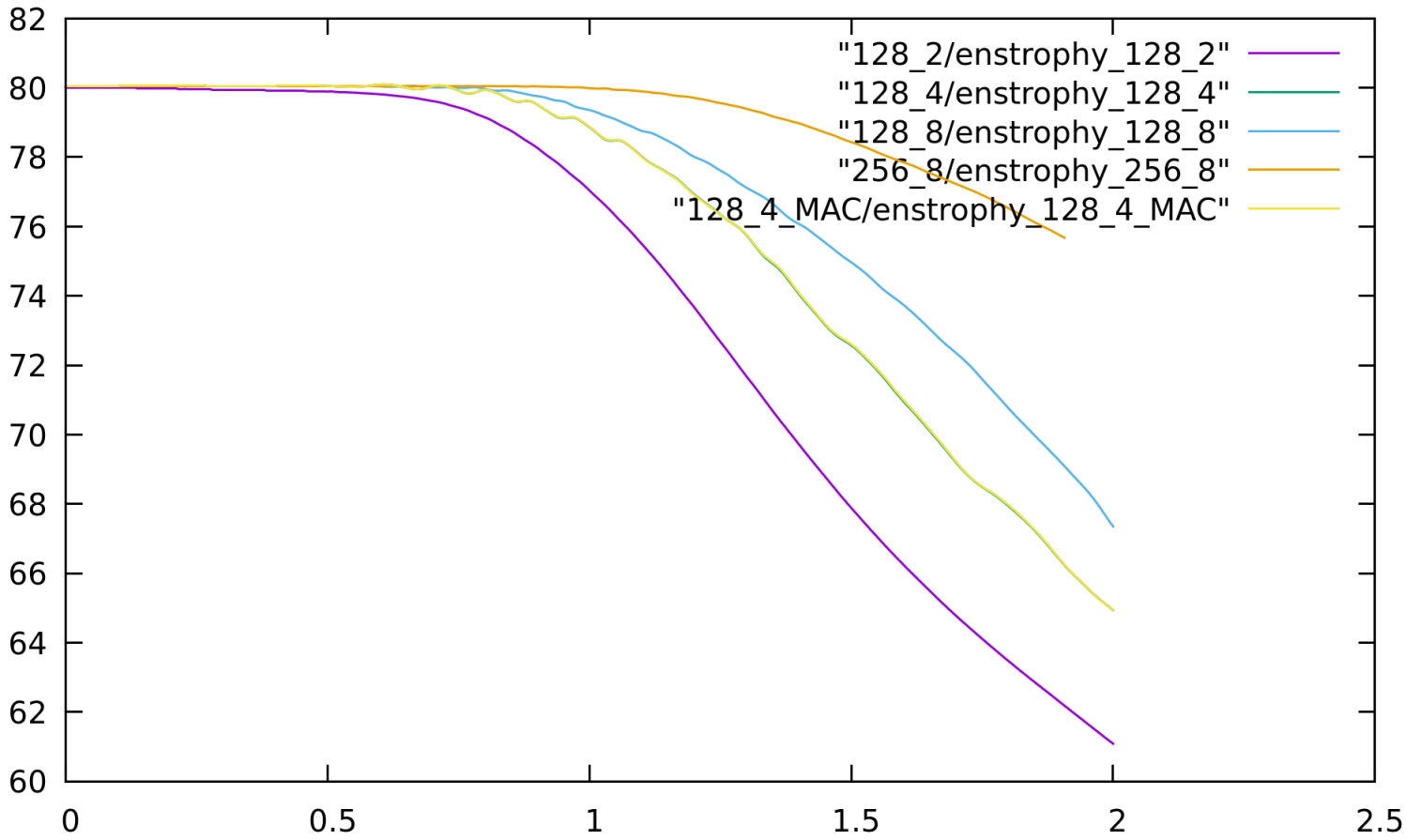

Double shear layer 2nd order 128x128

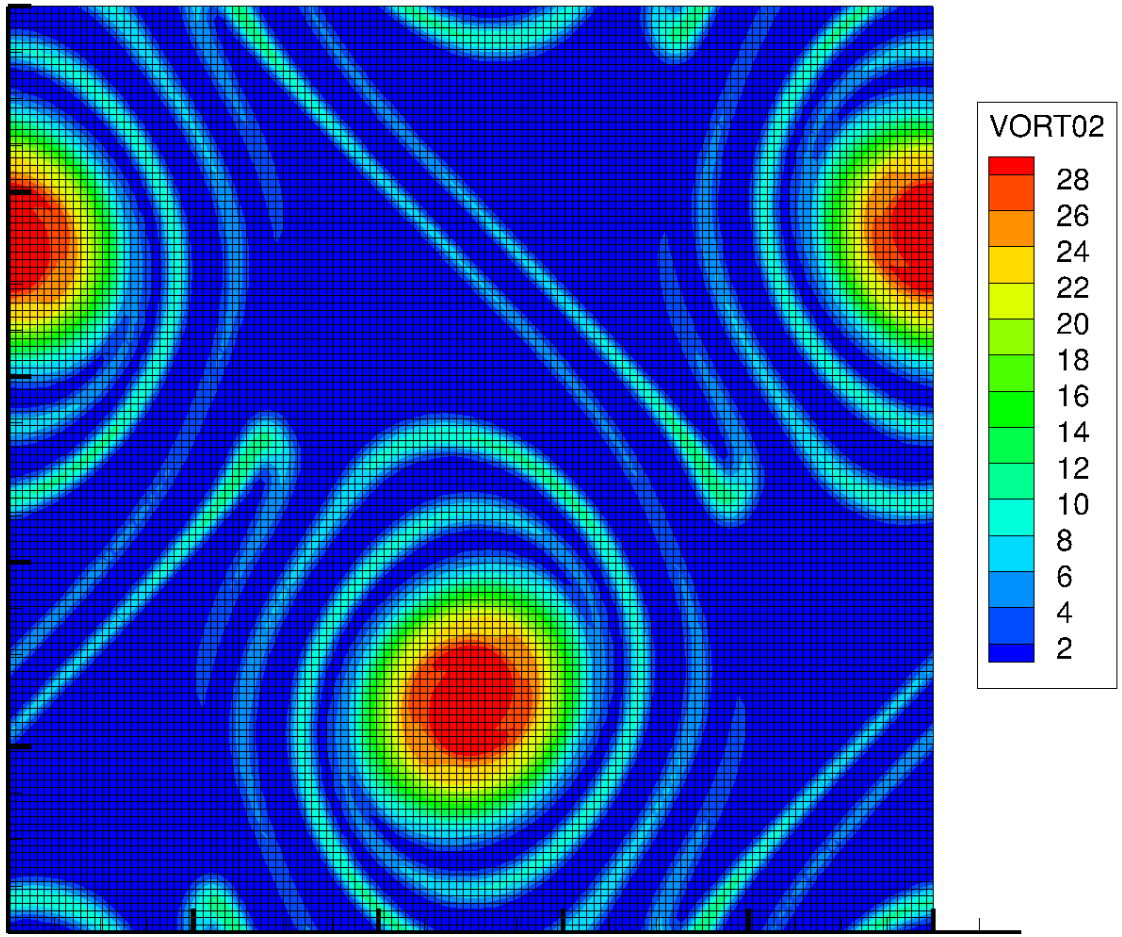

Double shear layer 4th order 128x128

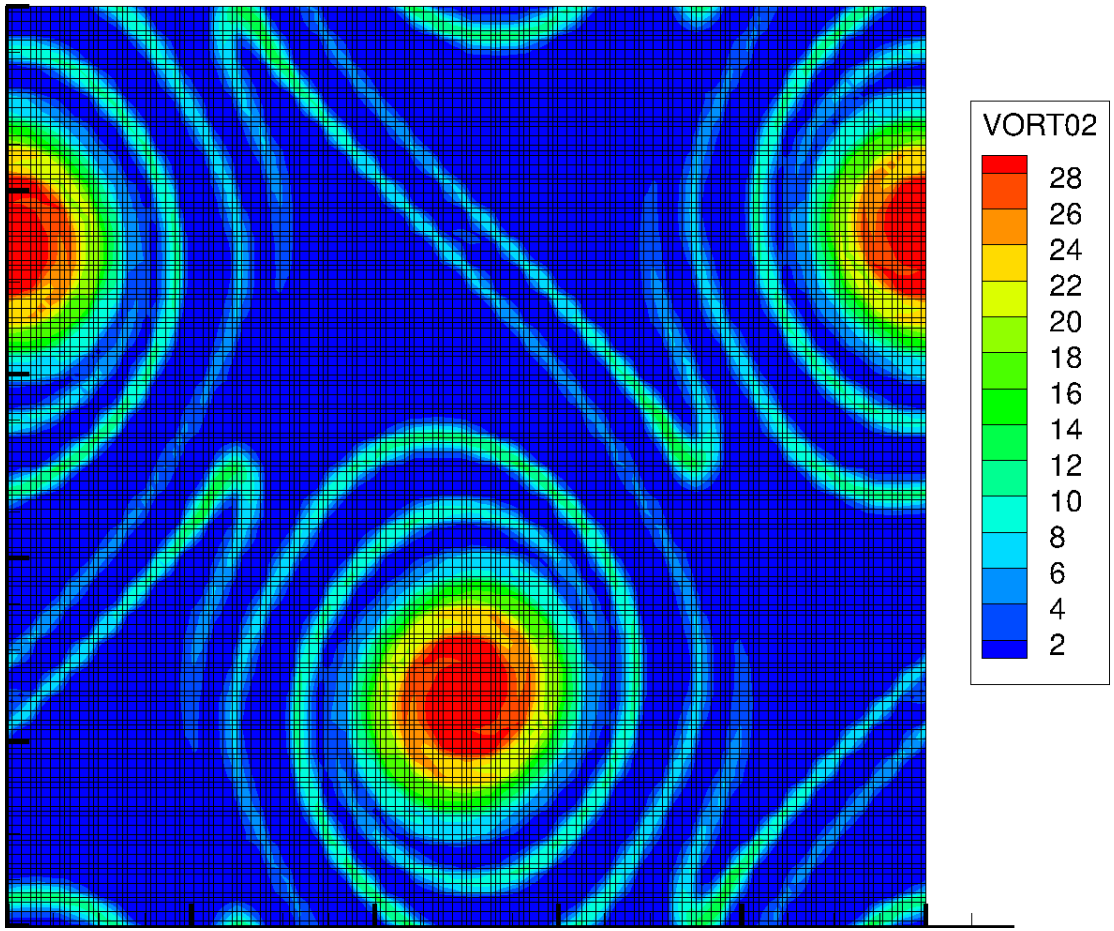

Double shear layer 4th order 128x128 vs 256x256

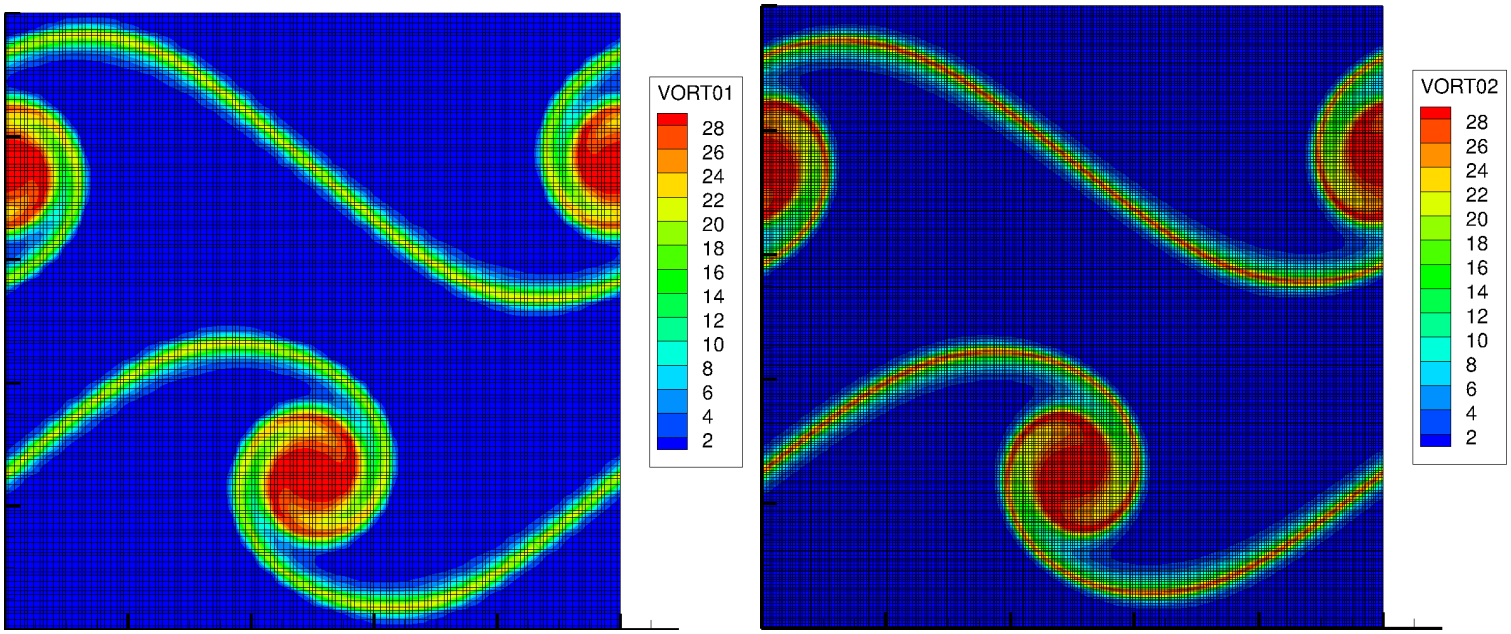

Initial vortex patch

At $t = 0$,

$$u = \alpha(r(\boldsymbol{x}))(y - y_0)$$

$$v = -\alpha(r(\boldsymbol{x}))(x - x_0)$$

$$r(\boldsymbol{x}) = \sqrt{(x - x_0)^2 + (y - y_0)^2}$$

Periodic boundary conditions, the following quantities should be constant with respect to time:

$$\int \boldsymbol{u} \cdot \boldsymbol{u}/2 dx \qquad \text{Kinetic Energy}$$

$$\int \boldsymbol{w} \cdot \boldsymbol{w} dx \quad \boldsymbol{w} = \nabla \times \boldsymbol{u} \qquad \text{Enstrophy}$$

Vortex patch, plot of enstrophy versus time

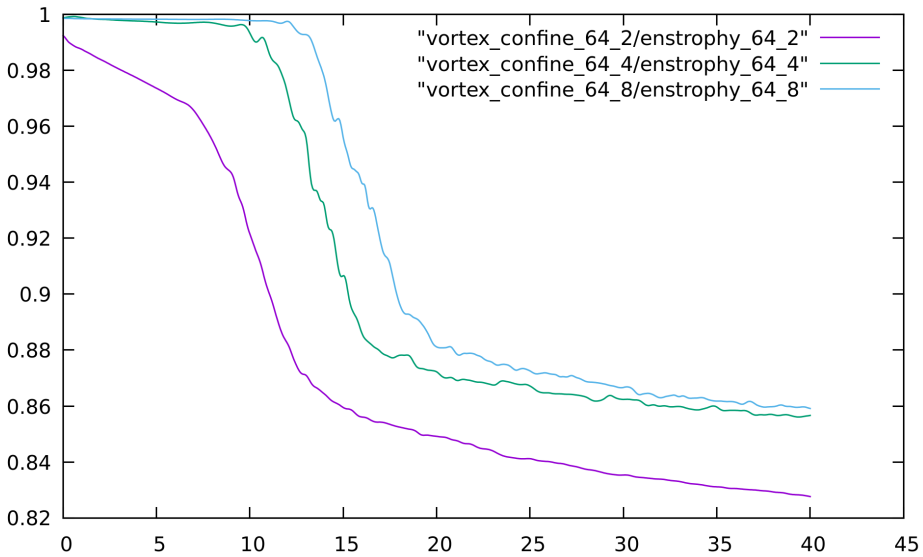

3D bubble

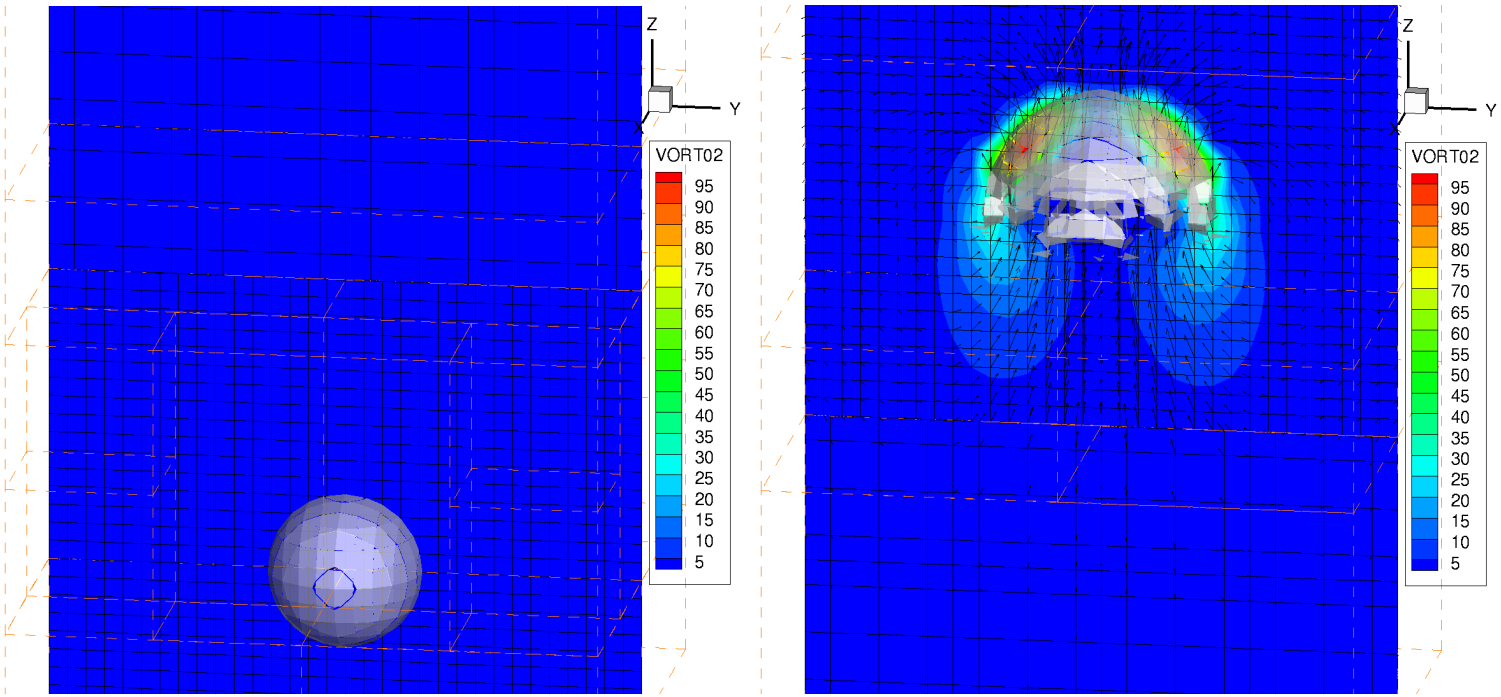
Z
Y
VORT02
95
90
85
80
75
70
65
60
55
50
45
40
35
30
25
20
15
10
5
Z
Y
VORT02
95
90
85
80
75
70
65
60
55
50
45
40
35
30
25
20
15
10
5

Liquid Jet in Gas Cross Flow (new method)

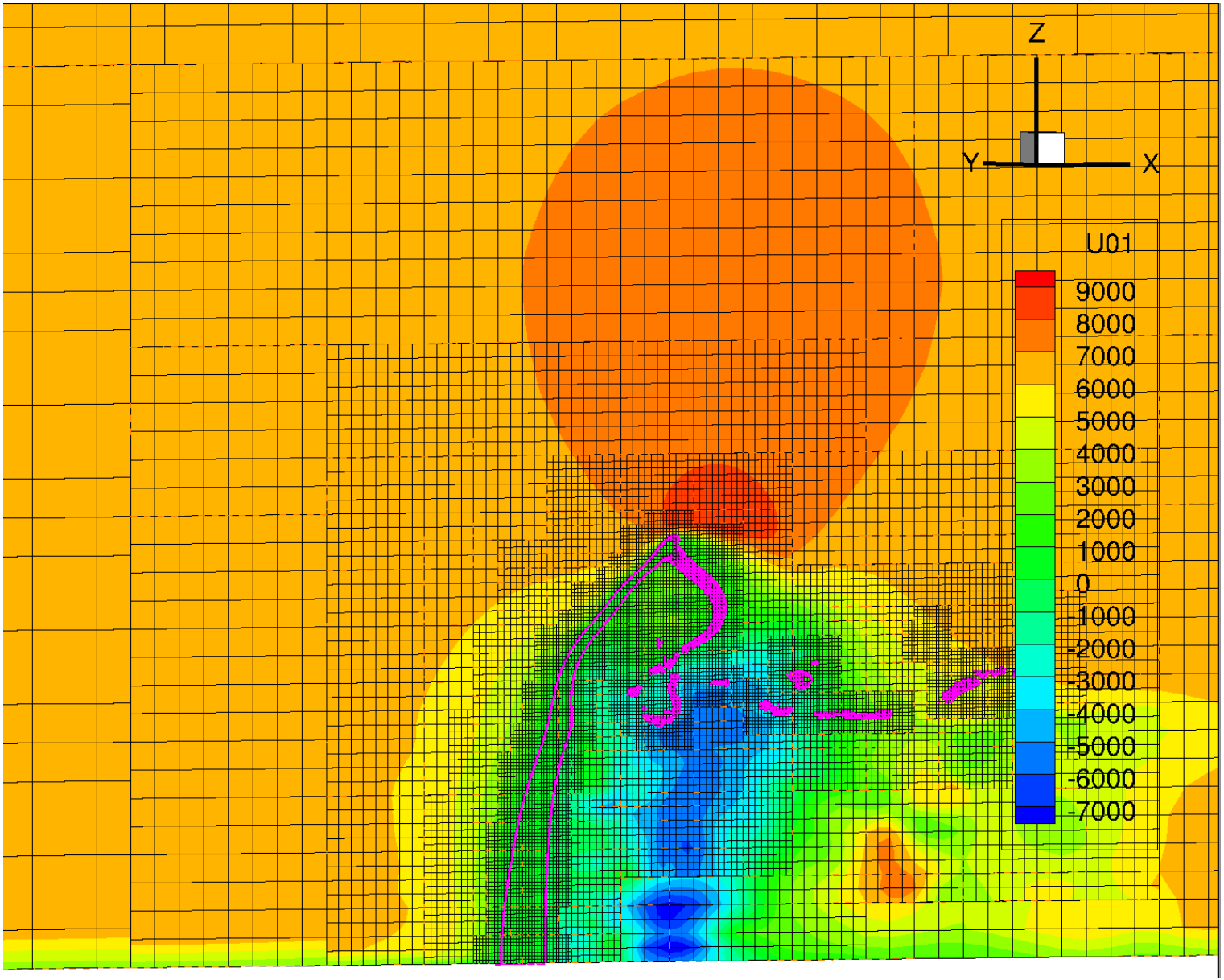

Liquid Jet in Gas Cross Flow (low order method)

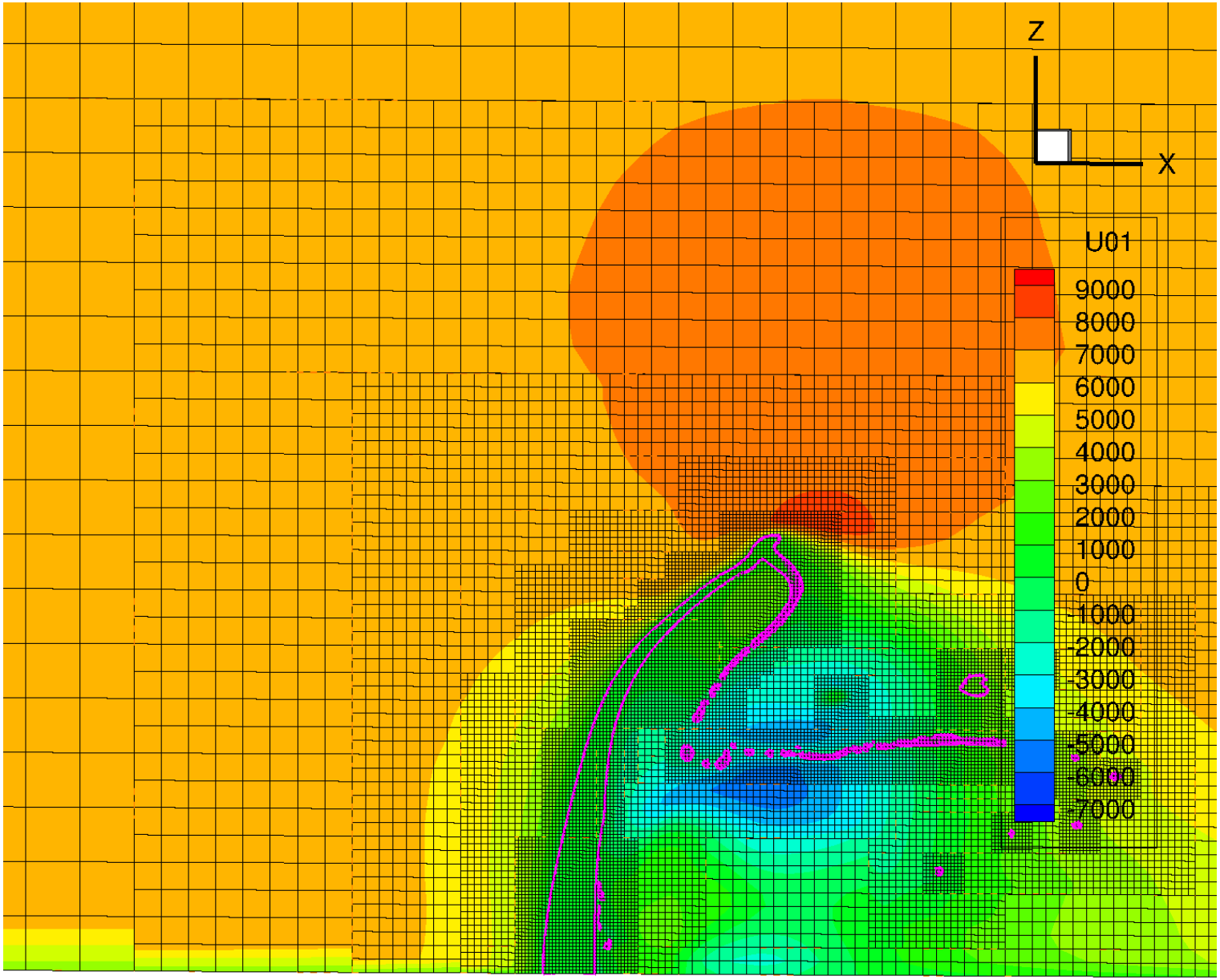

Nucleate Boiling

Journal of Computational Physics 300 (2015) 20–52

Contents lists available at ScienceDirect

Journal of Computational Physics

www.elsevier.com/locate/jcp

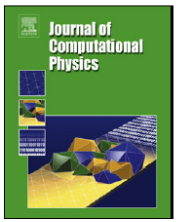

A depletable micro-layer model for nucleate pool boiling

Yohei Sato *, Bojan Niceno

Paul Scherrer Institute, Villigen PSI, 5232 Switzerland

ARTICLE INFO

Article history:
Received 21 December 2014
Received in revised form 4 July 2015
Accepted 24 July 2015
Available online 30 July 2015

Keywords:
Phase change
Interface tracking
Micro-layer model
Nucleate boiling
Conjugate heat transfer

ABSTRACT

A *depletable micro-layer* model has been developed for the simulation of nucleate pool boiling within the framework of Computational Fluid Dynamics (CFD) modeling using an interface-tracking method. A micro-layer model is required for the CFD simulation to take into account vaporization from the thin liquid film – called the micro-layer – existing beneath a growing vapor bubble on a hot surface. In our model, the thickness of the micro-layer is a variable defined at each discretized fluid cell adjacent to the heat-transfer surface; the layer decreases due to vaporization, and can finally disappear. Compared to existing micro-region models, most of them based on the concept of contact-line evaporation, as originally proposed by Stephan and Busse, and by Lay and Dhir, our model incorporates simplified modeling ideas, but can nonetheless predict the temperature field beneath the growing bubble accurately. The model proposed in this paper has been validated against measurements of pool boiling in water at atmospheric pressure. Specifically, the bubble principal dimensions and the temperature distribution over the heat-transfer surface are in good agreement with experimental data.

Nucleate Boiling

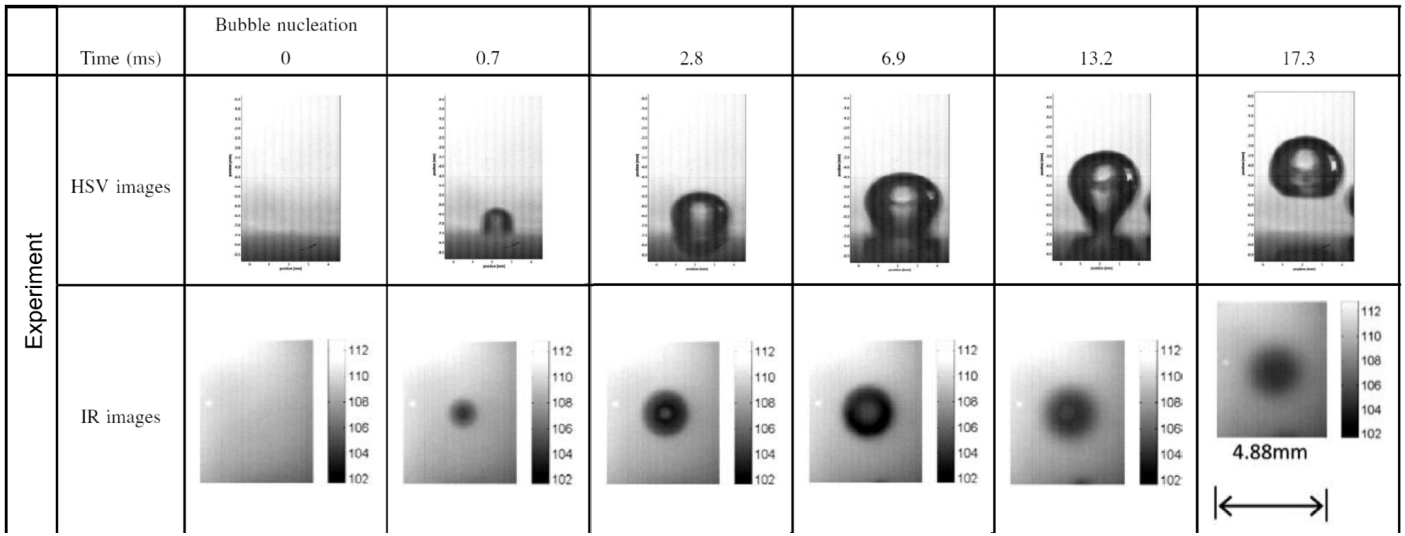

Nucleate Boiling

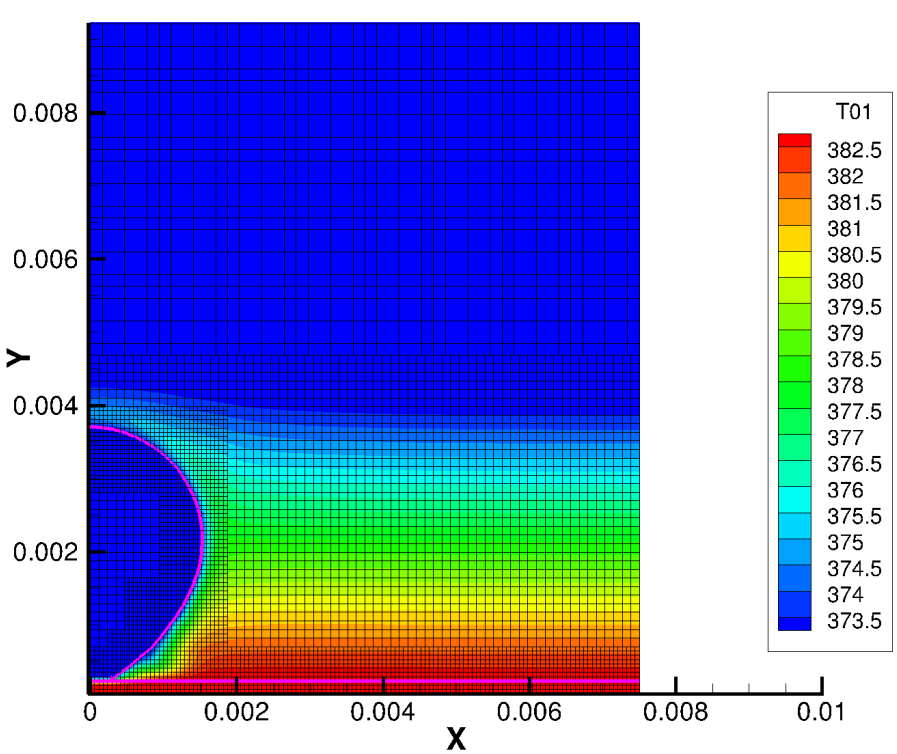

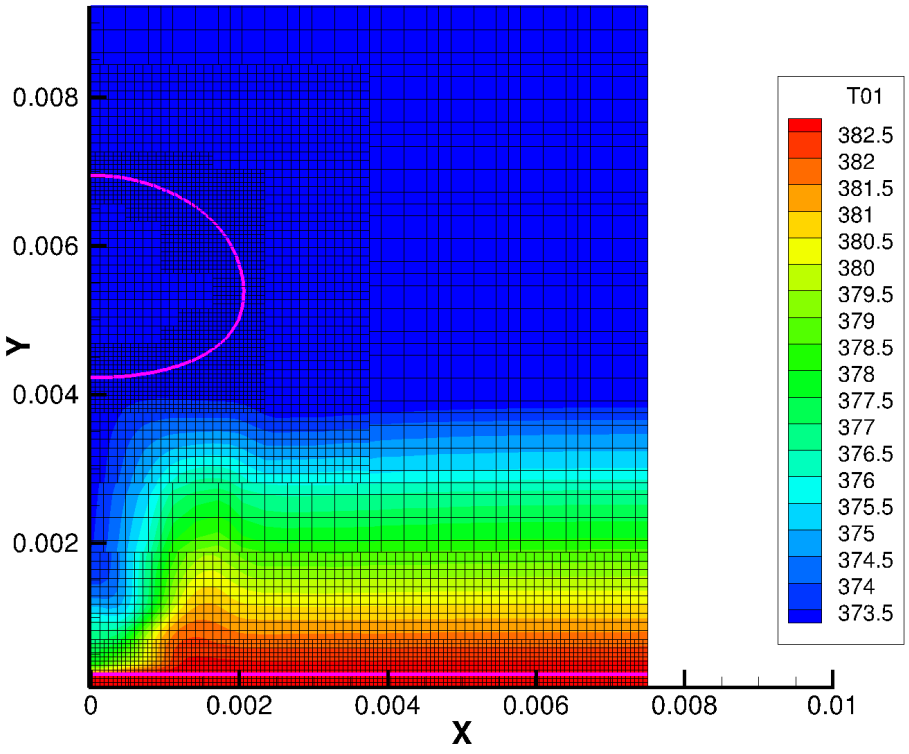

Differentially heated rotating annulus

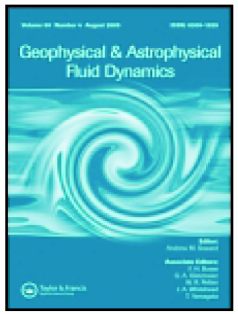

Taylor & Francis
Taylor & Francis Group

Geophysical & Astrophysical Fluid Dynamics

ISSN: 0309-1929 (Print) 1029-0419 (Online) Journal homepage: http://www.tandfonline.com/loi/ggaf20

Linear stability analysis for the differentially heated rotating annulus

Gregory M. Lewis & Wayne Nagata

To cite this article: Gregory M. Lewis & Wayne Nagata (2004) Linear stability analysis for the differentially heated rotating annulus, Geophysical & Astrophysical Fluid Dynamics, 98:2, 129-152, DOI: 10.1080/0309192042000204004

To link to this article: http://dx.doi.org/10.1080/0309192042000204004

Differentially heated rotating annulus

$$\frac{\partial \mathbf{u}}{\partial t} = \nu \nabla^2 \mathbf{u} - 2\Omega \mathbf{e}_z \times \mathbf{u} + (g\mathbf{e}_z - \Omega^2 r \mathbf{e}_r)\alpha(T - T_0) - \frac{1}{\rho_0}\nabla p - (\mathbf{u} \cdot \nabla)\mathbf{u}, \tag{4}$$

$$\frac{\partial T}{\partial t} = \kappa \nabla^2 T - (\mathbf{u} \cdot \nabla)T, \tag{5}$$

$$\nabla \cdot \mathbf{u} = 0, \tag{6}$$

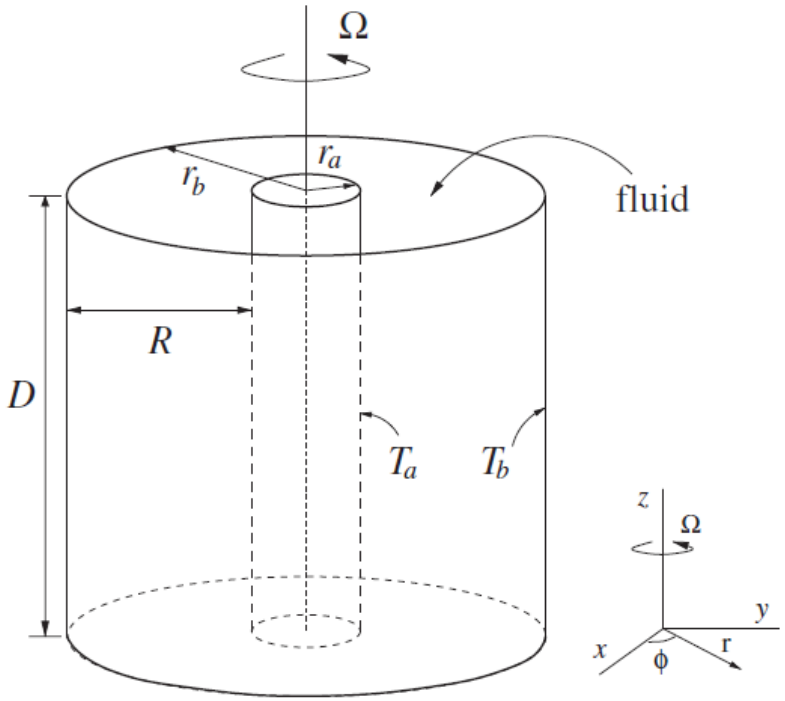

FIGURE 1 The differentially heated rotating annulus experiment, where the annulus is rotated at rate Ω and the inner wall is held at the fixed temperature T_a and the outer wall at temperature T_b, creating a differential heating. r_a and r_b are the radii of the inner and outer cylinders, $R = r_b - r_a$, and D is the height of the annulus.

Dynamics of Baroclinic Fluid Systems

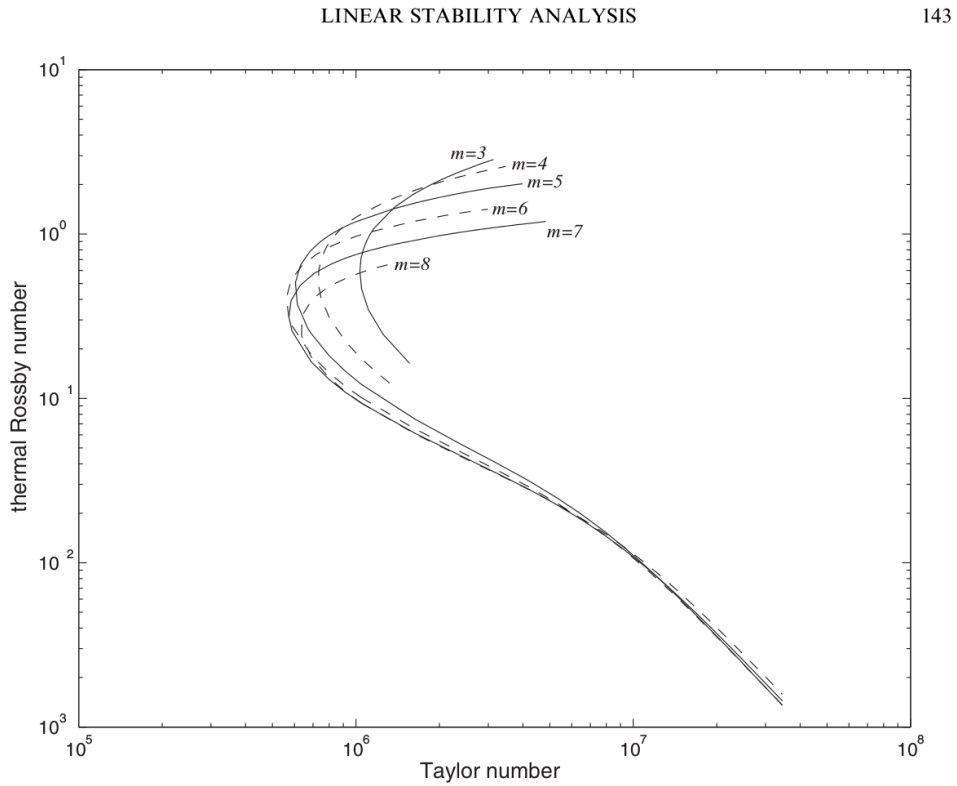

FIGURE 3 Neutral stability curves are plotted for the wave numbers $m = 3$ to $m = 8$. The curves are calculated by finding the parameter values where, for each m, the eigenvalues of (23) all have negative real part except one with zero real part. The curves are plotted on a log–log graph of thermal Rossby number *versus* Taylor number.

Taylor number: $4\Omega^2 R^4/\nu^4$

Thermal Rossby number: $\frac{\alpha g D \Delta T}{\Omega^2 R^2}$

Differentially heated rotating annulus

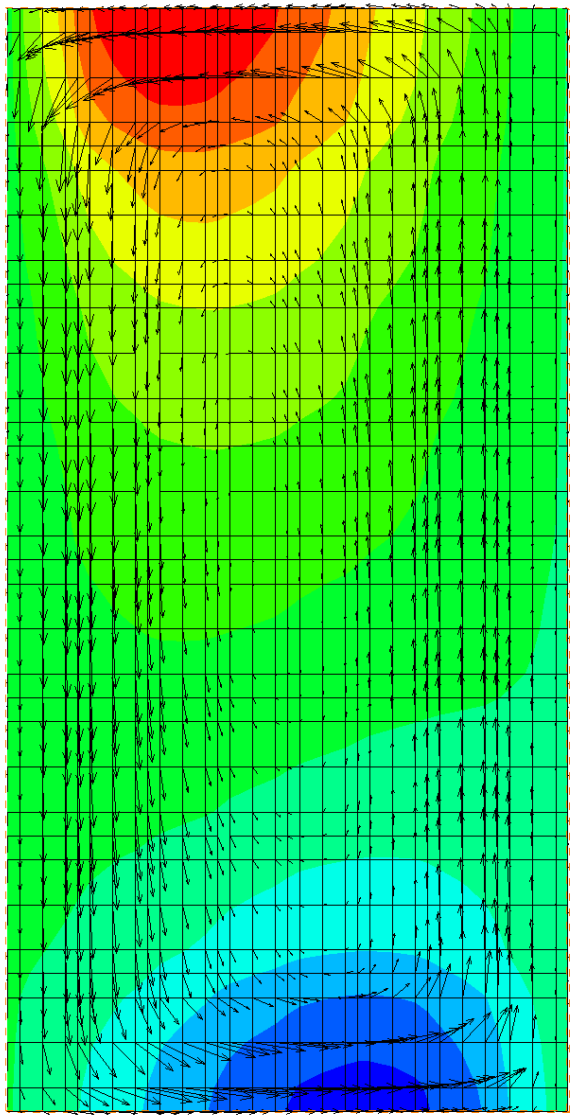

Conclusions and Future Work

- Our methodology is very good at approximating solutions to multiphase flow problems, taking into account contact line dynamics, phase change, vortical structures, and complex deforming boundaries, but, . . . ,
- for most practical problems, some kind of data assimilation technique (satellite data, experimental data, CAD/CAM data) and uncertainty quantification technique must be developed too. We are working on this now, using AMReX as a software infrastructure.